Tellus
SERIES A
DYNAMIC
METEOROLOGY
AND OCEANOGRAPHY
PUBLISHED BY THE INTERNATIONAL METEOROLOGICAL INSTITUTE IN STOCKHOLM

Tellus (2010), 62A, 411–434
Printed in Singapore. All rights reserved

TELLUS

Climatology of the Nordic (Irminger, Greenland, Barents, Kara and White/Pechora) Seas ice cover based on 85 GHz satellite microwave radiometry: 1992–2008

By S. KERN[1]*, L. KALESCHKE[1] and G. SPREEN[1,2], [1]*Centre for Marine and Climate Research, Institute of Oceanography, University of Hamburg, Bundesstr. 53, D-20146 Hamburg, Germany*; [2]*Jet Propulsion Laboratory, California Institute of Technology, Pasadena CA, USA*

(Manuscript received 16 July 2009; in final form 1 April 2010)

ABSTRACT

The ice cover of the Arctic peripheral seas bordering the Northern North Atlantic is examined for 1992–2008 using the ARTIST Sea Ice (ASI) algorithm applied to derive the sea ice concentration from 85 GHz SSM/I measurements. Our analysis reveals a 2 months longer ice-free season in the Irminger Sea (IS), and reductions in ice area and extent between 1992–1999 and 2000–2008 by 10–20% during winter and 30–55% in summer. Barents Sea (BS) ice-cover anomalies (ICA) persist twice as long as ICA in the other regions. Early winter ICA in region IS are correlated to late summer/fall Greenland Sea (GS) ICA. Summertime GS and wintertime IS ICA are correlated to winter Fram Strait ice-area flux anomalies. The wintertime GS ice-cover decrease is associated with less Is Odden events. Our analysis suggests a large-scale, interregional ocean–ice–atmosphere feedback mechanism involving regions BS, Kara (KS) and White/Pechora Sea (WPS). To understand this mechanism the current and preceding general atmospheric circulation, associated variations in Arctic Ocean ice export and oceanic heat advection are needed. However, our results suggest (1) BS ICA could play a key role to predict subsequent KS ICA and (2) anomalous Arctic Ocean ice export into BS could trigger long-lasting BS ICA.

1. Introduction

The Arctic sea ice cover is decreasing in terms of its extent (Comiso et al., 2008) and its thickness (Haas et al., 2008; Kwok et al., 2009), and it has become younger (Rigor and Wallace, 2004). This has implications for the sea ice and liquid freshwater export out of the Arctic into the Greenland and Barents Seas (Aagaard and Carmack, 1989; Kwok et al., 2004, 2005; Holfort and Meincke, 2005; Dickson et al., 2007; Kwok, 2009; Spreen et al., 2009), thereby on water mass modification in these seas (Visbeck et al., 1995; Gerdes et al., 2003; Karstensen et al., 2005) and the Northern North Atlantic, and subsequently on the meridional overturning circulation (Dickson et al., 1988, 2007; Jungclaus et al., 2005).

In this paper the sea-ice cover of the Arctic peripheral seas bordering the Northern North Atlantic is examined, i.e. the Irminger Sea (IS), Greenland Sea (GS), Barents Sea (BS), White/Pechora Sea (WPS) and Kara Sea (KS). Observations about the variability and trends in the sea-ice cover of these regions for the years 1979–2006 can be found in Parkinson and Cavalieri (2008), however, with regions IS and GS, and BS, WPS and KS being considered together. In the GS the so-called 'Is Odden', an ice tongue of predominantly thin ice that typically extends from the West of Jan Mayen to the Northeast (Comiso et al., 2001) is of particular interest. Wilkinson and Wadhams (2003) underlined the role of this feature and the associated ice production for the water mass modification in the GS via deep oceanic convection (Latarius and Quadfasel, 2010). The role of sea-ice formation and melting in the BS is of equal importance because it influences the Barents Sea Inflow (Schauer et al., 2002; Gerdes et al., 2003; Sundfjord et al., 2008). Ice exported out of region KS is partly imported into regions BS and GS via the Arctic Ocean (Pfirman et al., 1997, 2004; Kwok, 2009). Sea-ice formation associated with brine release in the KS helps maintaining the cold Arctic halocline layer (Winsor and Björk, 2000). Finally, ice conditions in the IS influence the salinity of the surface water layer in the Labrador Sea, and thereby have an impact on deep convection (Deshayes et al., 2007).

Rodrigues (2006, 2008) discuss sea-ice area, sea-ice edge and length of the ice-free season in the Russian Arctic for years 1979–2007. As part of the Russian Arctic changes in the KS, BS and WPS are discussed. Between 1979 and 2007 they observe

*Corresponding author.
e-mail: stefan.kern@zmaw.de
DOI: 10.1111/j.1600-0870.2010.00457.x

a strong sea-ice area reduction in the BS all year round (mean: −37%) and a strong reduction in the KS during summer months (July, August, September: −46%; BS: −55%). The WPS exhibits the most pronounced rise in the length of the ice-free season of 105 d between 1979 and 2006.

Already before our observational period the Nordic Seas sea-ice extent declined. Divine and Dick (2006) find a continuous negative trend of the ice-edge position in the Nordic Seas for April–August 1750–2002 superimposed by oscillations of the ice-edge position with periods of 20–30 yr (more prevalent in the BS) and of 60–80 yr (more prevalent in the GS). Vinje (2001) find a 33% reduction in sea-ice extent during the 135 yr long period 1864–1998. Their definition of Nordic Seas comprises the Greenland, Iceland, Norwegian, Barents and western Kara Sea. In contrast to recent decades with enhanced atmospheric temperatures this preceding sea-ice reduction can mainly be attributed to a temperature increase of about 1 °C of the upper ocean layer (Vinje, 2001).

For the 1953–1984 period Mysak and Manak (1989) find a strong decadal cycle of the sea-ice extent in both the combined IS/GS and BS/WPS/KS regions. They speculate that this time-scale could be set by the similar circulation time scale of the subarctic gyre in the North Atlantic. Due to the only 17 yr length of the here presented time series we do not expect to resolve this decadal variability. Using a cross-correlation analysis similar to the one applied in Section 3.4 of this study Mysak and Manak (1989) show that a positive sea-ice extent anomaly propagated in about 4 yr from the Greenland Sea to the Labrador Sea between 1968 and 1972 associated with the Great Salinity Anomaly (Dickson et al., 1988).

Changes in the Nordic Seas sea-ice cover do not only influence the physical interactions between ocean, atmosphere, and sea-ice as, for example, heat fluxes or the already mentioned water mass modification. But these changes also interfere with the (1) ecosystems depending on sea-ice, (2) human activities in the Nordic Seas as, for example, shipping routes and drilling for natural resources and (3) the people living in this part of the Arctic region (ACIA, 2005; Arrigo et al., 2008; Rysgaard et al., 2009).

This paper looks at the variability of the sea-ice cover in the five above-mentioned regions by means of satellite microwave radiometry using brightness temperatures measured by the Defence Meteorological Satellite Program (DMSP) Special Sensor Microwave/Imager (SSM/I) instrument. Instead of using standard ice concentration products provided with the NASA-Team algorithm (NTA) or the Comiso-Bootstrap algorithm (CBA), which both use the low-frequency channels (19 and 37 GHz) of the SSM/I (Comiso et al., 1997), the present paper is based on the ARTIST Sea Ice (ASI) concentration algorithm (Kaleschke et al., 2001). The ASI algorithm uses data of the 85.5 GHz channels of the SSM/I and thereby permits a grid resolution of 12.5 km × 12.5 km. This higher spatial resolution compared to CBA and NTA is of especial advantage for monitoring the sea ice in small marginal seas like the WPS region of this study.

We examine the sea-ice concentration distribution for the IS, GS, BS, WPS and KS Seas for the years 1992–2008. The goal is to answer the following questions:

(i) Did the annual cycle of sea-ice area and extent in these regions change recently?

(ii) What are the differences and/or similarities in sea-ice area and extent anomalies observed in these regions?

(iii) Are sea-ice area and extent anomalies observed in one of these regions linked to those observed in the other mentioned regions?

2. Data sets and methodology

2.1. Sea-ice concentration retrieval

2.1.1. ASI-algorithm. We use daily sea-ice concentration derived from the difference of the vertically v and horizontally h polarized brightness temperatures, Tb (polarization difference $P = Tb_v - Tb_h$) measured by the SSM/I at a frequency of 85.5 GHz. P is the polarization difference at 85 GHz, which is about 2–20 K for most sea-ice types and one order of magnitude larger for open water (NORSEX Group, 1983; Onstott et al., 1987), and can thus be used to infer the partial sea ice coverage within the sensor's field-of-view (FOV), that is, the sea-ice concentration. The ASI algorithm is based on the approach of Svendsen et al. (1987), has been developed by Kaleschke et al. (2001), and has been further refined and modified for 89 GHz data of the Advanced Microwave Scanning Radiometer by Spreen et al. (2008). The FOV of the SSM/I at 85.5 GHz is 15 km × 13 km, whereas the FOV at 19 and 37 GHz is 69 km × 45 km and 37 km × 29 km, respectively. ASI ice concentration based on SSM/I data are thus on a 12.5 km × 12.5 km grid. CBA and NTA ice concentration data based on SSM/I are on a 25 km × 25 km grid, although the resolution of the 19 GHz SSM/I channels is much coarser.

The optical depth of level thin sea ice grown under calm conditions is about an order of magnitude smaller at 85 GHz (2–3 mm) compared to 19 or 37 GHz (10–30 mm) (Grenfell et al., 1998). As a consequence the observed brightness temperature at 85 GHz in comparison to 19 or 37 GHz is solely influenced by the sea ice dielectric properties already at a smaller ice thickness. Or in other words: 85 GHz brightness temperatures saturate earlier at values typically observed over thick level sea ice (Shokr et al., 2009). Therefore, ASI algorithm ice concentrations are higher in regions covered by thin sea ice compared to CBA and NTA algorithm ice concentrations in theory. Note that this might become invalid for pancake ice, because of its different growth and thus desalination mechanism causing different dielectric and surface properties compared to level thin sea ice. Attention has also to be paid in case that the ice surface becomes wet (Shokr et al., 2009).

A disadvantage of using the 85 GHz SSM/I channels is the availability of the data: The first two SSM/I instruments aboard DMSP-f8 and -f10 suffered from a mal-function of the 85 GHz channels and from an imperfect orbit, respectively, so that the analysis of a continuous time series of SSM/I 85 GHz data is recommended starting with data from the SSM/I aboard DMSP-f11 (November 28, 1991). Consequently, in the present paper ASI ice concentration data of the period 1992–2008 are investigated.

The ice concentration data used in this paper are processed operationally at the ESA branch CERSAT/IFREMER, Brest, France, using the ASI-algorithm applied to 85 GHz SSM/I data and the weather filters described below. The data is updated following data distribution by the NSIDC. The data is quality checked and is available via anonymous ftp: ftp://ftp.ifremer.fr/ifremer/cersat/products/gridded/psi-concentration/data/.

2.1.2. Treatment of the weather influence. Using 85 GHz data for sea-ice concentration retrieval requires a proper treatment of the weather influence on the measured brightness temperatures (Kaleschke et al., 2001; Kern, 2004; Spreen et al., 2008). The atmospheric water vapour, the cloud liquid water content as well as wind-induced roughening of the water surface decrease the value of P and can thus cause spurious sea-ice concentrations over open water (Kaleschke et al., 2001; Garrity et al., 2002; Kern, 2004). In order to mitigate this influence weather filters are applied. These are based on the approaches by Gloersen and Cavalieri (1986) and Cavalieri et al. (1995), and use the low-frequency SSM/I channels (19, 22 and 37 GHz) to filter out areas influenced by cloud liquid water and water vapour, respectively. This way most spurious ice over open water is removed. More details can be found in Spreen et al. (2008).

Sea-ice concentration estimates based on the ASI algorithm have been compared against other ice concentration data based on satellite microwave radiometry by means of using independent data such as satellite and airborne visible imagery, spaceborne synthetic aperture radar data, and ship-based observations (Kaleschke et al., 2001; Garrity et al., 2002; Kern et al., 2003; Andersen et al., 2007). These studies demonstrated the capability of the ASI algorithm to resolve more details in the ice concentration distribution than is possible using the CBA or the NTA with similar accuracy. In particular, for high ice concentrations usage of near 90 GHz brightness temperatures outperforms ice-concentration retrieval algorithms where the information on the ice concentration is mainly based on lower-frequency brightness temperatures for various reasons. This has been explicitly demonstrated in Andersen et al. (2007).

Despite the various weather filters used, an animation of daily ASI algorithm sea-ice concentration data reveals that still a few residual spurious sea-ice patches exist over open water. Moreover, the above-mentioned weather filters are not designed to correct for the weather influence over sea ice. Consequently, higher (lower) than average cloud liquid water and/or water vapour values over sea ice may cause an ice-concentration over- (under-) estimation, particularly over the marginal ice zone (MIZ). Apart from this direct also an indirect weather influence exists. This is the variation of sea-ice surface (radiometric) properties by weather-induced changes in snow temperature, wetness, and morphology as well as in the fraction of new and/or deformed sea ice in the FOV. Both the direct and the indirect weather influence can cause widespread false sea-ice concentration variations. Since these are associated with fast-moving (relative to the sea-ice motion) low-pressure systems, filtering in the time-domain can mitigate these weather effects. A sliding Median-filter (Jähne, 1997) with a width of 5 d is applied to the entire ASI algorithm sea-ice concentration data set provided by IFREMER. This filter replaces the centre value of the odd-numbered vector (5 d) of ASI sea-ice concentrations with the centre value of the same but rank-ordered vector.

The effect of this filtering is illustrated in Fig. 2 which shows a pair of unfiltered and Median-filtered ASI ice concentration data for February 15, 2007 in our region of interest (see Fig. 1). Figure 2a shows two patches of residual spurious ice-concentrations

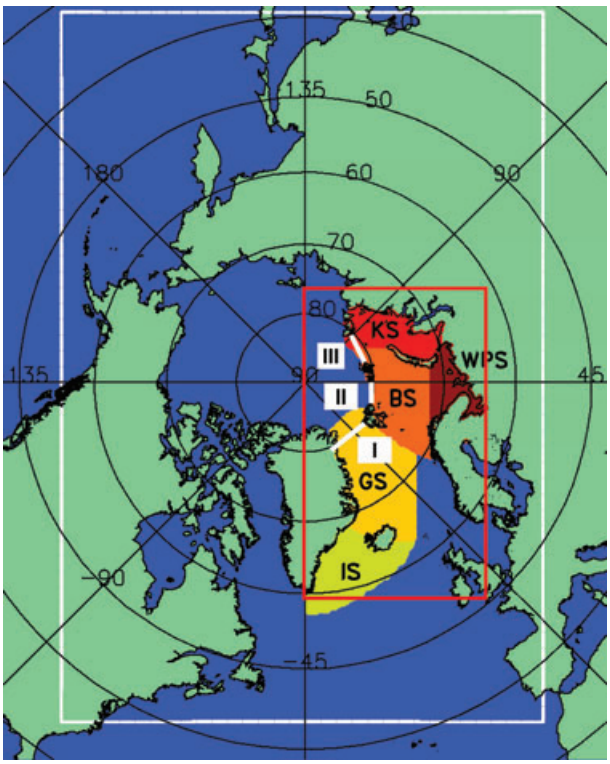

Fig. 1. Map of the Arctic Ocean and its peripheral Seas. The white rectangle denotes the area for which ASI ice concentrations are calculated in general. The five regions of interest: Irminger Sea (IS), Greenland Sea (GS), Barents Sea (BS), White/Pechora Sea (WPS) and Kara Sea (KS) are shaded in different colours. The red rectangle denotes the area for which examples of the difference between Median-filtered and unfiltered ASI ice concentration maps are shown in Figs. 2. Thick white lines denoted by I, II and III mark the flux gates mentioned later.

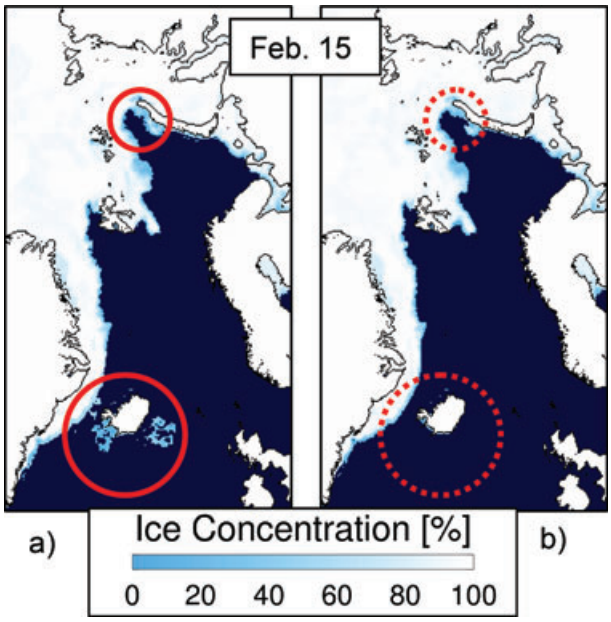

Fig. 2. One pair of daily raw (a) and Median-filtered (b) ASI algorithm sea-ice concentration maps for February 15, 2007 for the area denoted by the red rectangle in Fig. 1. Red circles denote areas where the Median-filter removes spurious ice concentrations over open water and at the ice edge.

south and west of Iceland which are successfully removed by the filter (Fig. 2b).

A disadvantage of the median filter is, that fast and short-lived processes like sudden polynya opening and closing or temporary shifts of the ice edge are not well represented in the obtained time series. For the here considered long term and monthly changes these filtered processes are of negligible importance (see also Section 2.2.2).

2.2. *Sea-ice concentration anomalies, sea-ice area and extent*

2.2.1. Deriving the quantities. Daily maps of the sea-ice concentration are used to calculate monthly average sea-ice concentrations for each grid cell. The daily sea-ice concentration maps are also used to calculate the average daily sea-ice concentration for each grid cell for the periods 1992–1999, 2000–2008 and 1992–2008. These average daily sea-ice concentrations are used to calculate daily sea-ice concentration anomalies. These anomalies are subsequently averaged over 1 month to obtain monthly average sea-ice concentration anomalies (see Figs. 5 and 6) and their temporal standard deviations for each grid cell.

By using the grid cell area of each grid cell as provided by the National Snow and Ice Data Centre (NSIDC, http://nsidc.org/data/polar_stereo/tools_geo_pixel.html) and the region mask (Gloersen et al., 1992) (NSIDC, http://nsidc.org/data/polar_stereo/tools_masks.html) the monthly average sea-ice area and extent is calculated from the monthly average sea-ice concentration data. The region mask is modified such that the two original regions Greenland Sea, and Kara and Barents Sea (Gloersen et al., 1992) are split to become five regions: IS, GS, BS, WPS and KS (see Fig. 1). The sea-ice extent is considered as the total area of all grid cells with at least 15% ice concentration. The sea-ice area is considered as the ice-concentration weighted total area of all grid cells with at least 15% ice concentration. The monthly average sea-ice area and extent values are used to compute their average annual cycle for the same periods mentioned above. These annual cycles are subsequently used to calculate time-series of the monthly average sea-ice area and extent anomalies.

2.2.2. Comparison with other data. In order to check, whether the sea-ice area and extent values based on ASI algorithm sea-ice concentrations differ from values based on other coarse-resolution algorithms, ASI algorithm data have been resolution-reduced to match the grid-cell size of, for example, the CBA data: 25 km × 25 km. Subsequently, sea-ice extent and area is calculated and compared with the same quantities derived from CBA data obtained from the NSIDC for the period 1992–2007 (Comiso, 1999). Furthermore the difference CBA minus ASI monthly ice area and extent is computed. Finally, in order to check whether this difference perhaps takes an absolute maximum value in a certain month we calculated histograms of the distribution of these differences over the months of a year for 1992–2007.

Figure 3 shows the results of this examination. The best agreement between CBA- and ASI-based ice extent and area is observed in regions GS, BS, and KS (Figs. 3c, e and g) with regression-line slopes close to unity (0.986–1.068) and squared linear correlation coefficients (R^2) close to or above 0.99. For regions IS and WPS (Figs. 3a and i) agreement between CBA and ASI ice area and extent is still reasonable but worse than in the other three regions; regression-line slopes take values around 1.1, and R^2 takes values between 0.96 and 0.99. Particularly the scatterplot for region WPS (Fig. 3i) shows considerable differences between CBA and ASI once area and extent fall below 2×10^5 km^2.

The differences CBA minus ASI ice area and extent shown in Fig. 3, right-hand column, are on average all positive in accordance with the positive biases and regression-line slopes larger than unity given in Fig. 3, left-hand column. The largest average ice-area differences are observed for regions KS, GS and BS; the largest average ice-extent differences are found in regions GS and BS. This is mainly due to their larger ice covered area compared to IS and WPS (Fig. 3, left-hand column). Note that the 12-month running mean ice-area (ice-extent) differences seem to have a weak negative trend in regions BS and GS (Figs. 3d and f).

The observed overestimation of ice-area and extent by CBA relative to ASI is in line with our expectations for two reasons. At first, the tie points used by the ASI algorithm applied here are

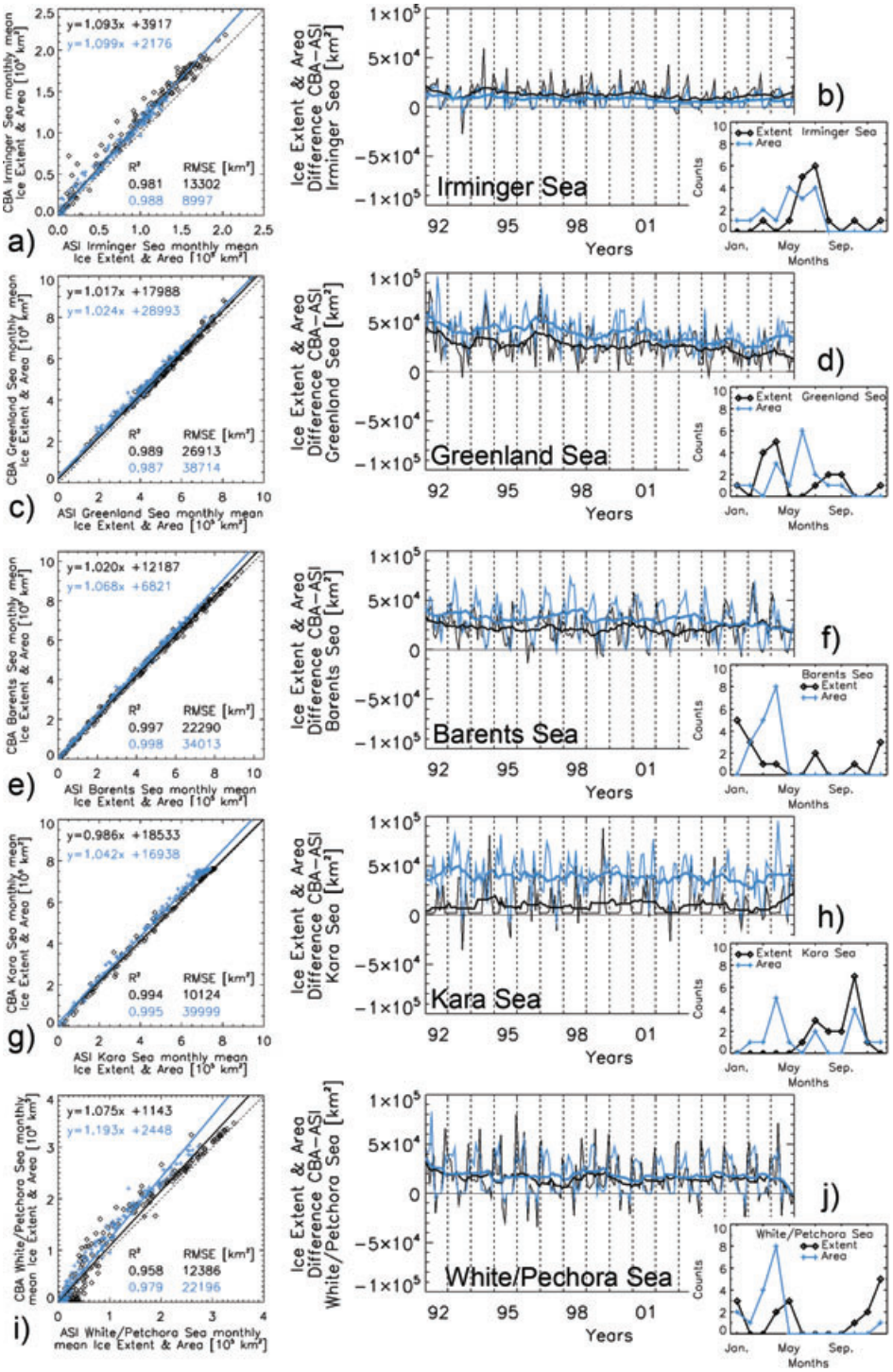

Fig. 3. Left-hand column: comparison between average monthly sea-ice extent (black symbols) and area (blue symbols) based on the ASI algorithm (*X*-axis) and the Comiso-Bootstrap algorithm (*Y*-axis) for 1992–2007 for (a) IS, (c) GS, (e) BS, (g) KS and (i) WPS (see Fig. 1). Dotted black lines indicate perfect agreement between data of the two algorithms. Solid lines coloured as the symbols denote the linear regression line between data of both algorithms; the equations of these lines are given in the top left of each image; in the bottom right the linear Pearson correlation coefficient is shown together with the RMSE of the regression line. Note different axis scaling. Right-hand column: Time series of the difference CBA minus ASI algorithm based monthly mean sea-ice extent (black) and area (blue) for (b) IS, (d) GS, (f) BS, (h) KS and (j) WPS. The thick lines denote a 12-month running mean. Note that *Y*-axes are scaled similarly for these images. The insert at each difference image shows the number of years within which the absolute maximum ice-extent and area difference occurred in the month displayed at the *X*-axis.

estimated with the aid of NTA ice concentrations. The NTA is known to underestimate the sea-ice concentration with respect to the CBA (Comiso et al., 1997). Second, the finer spatial resolution achieved with the ASI algorithm permits to identify more of the open water patches, leads, and polynyas even when the grid-cell size is matched with that of the CBA results. Consequently ASI ice concentrations tend to be below CBA ones and thus particularly the resulting ice area is smaller than the one obtained with the CBA. A good example is the histogram given in Fig. 3h): large CBA minus ASI ice-area differences occur most often in region KS in Apr. when the polynyas tend to widen. Another example is the histogram in Fig. 3d): the highest number of CBA minus ASI ice-area differences occur in region GS most often in June, when the leads and openings in the typically divergent ice stream along the Greenland coast do not freeze over again. Note that residual weather effects which are accounted for neither by the used weather filters nor the median filter would contribute to a negative rather than a positive CBA minus ASI ice-area and -extent difference.

The finer spatial resolution achieved with the ASI algorithm also reduces the degree with which the obtained ice concentration is contaminated by the influence of land on the observed *Tb*. This is illustrated by Figure 4. When taking the different FOV sizes into account, the land contamination of the observed *Tb* reaches at least as far as 50 km at 19 GHz (Fig. 4a); at 85 GHz the respective number is about 10 km (Fig. 4b). The sea-ice band along the coast of Greenland in region IS is often as narrow as a few ten kilometres. It is therefore likely that the observed difference between CBA and ASI ice-area and extent (Fig. 3b) is caused at least partly by the different land contamination. Note that the ASI algorithm permits to map sea ice closer to the coast and by this could capture this narrow sea-ice band more realistically (Fig. 4b). The CBA would likely show sea ice for all three selected grid cells in Fig. 4a) due to land contamination while in reality only one is covered by sea ice. This effect might also explain the differences between CBA and ASI ice area and extent in region WPS (Fig. 3j), while it is probably less important for regions GS and BS, because of their larger overall area and more extensive sea-ice coverage. Evidence for this is given by the histograms in Figs. 3h and j: In regions KS and WPS largest CBA minus ASI ice-extent differences occur in October (KS) and December (WPS), the months of freeze-up, which in these regions starts along the coasts, so that land contamination of the obtained ice-area and extent can be quite substantial.

Difference maps of the monthly average CBA and ASI ice concentration (CBA-ASI, not shown here) show a transition from positive differences in the MIZ (facing the open water) over negative differences in the MIZ (facing the pack ice) to differences close to zero over the pack ice. We explain this again with the finer spatial resolution possible with the ASI, which permits a much better representation of a compact ice edge (Kaleschke et al., 2001; Kern et al., 2003). In particular in regions BS and GS, where low-pressure systems moving along the ice edge cause a change between divergent and convergent ice situations, an algorithm based on coarse-resolution data (CBA) would achieve a less precise (1) average location of the ice edge and (2) across-MIZ ice-concentration gradient compared to an algorithm using finer resolved data. Histograms given for regions GS and BS in Figs. 3d and f) seem to confirm this, at least partly: months with the highest number of large CBA minus ASI

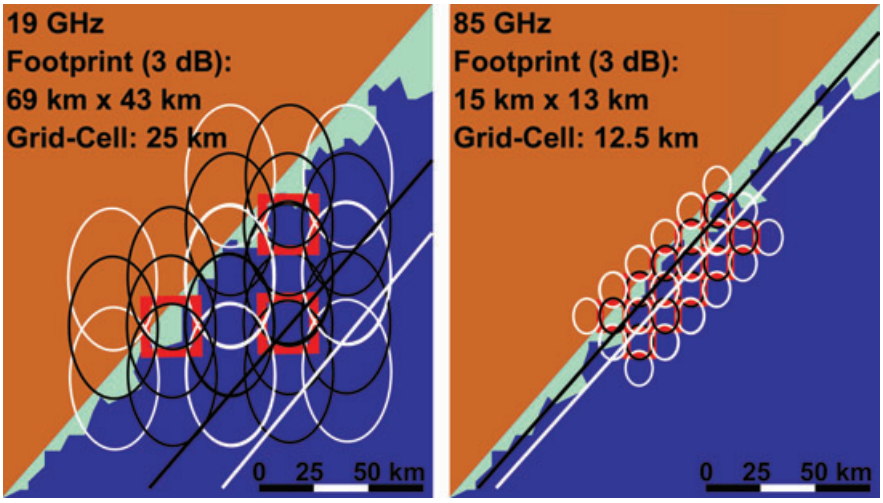

Fig. 4. Schematic sketch of a land-sea ice-water distribution typical for Southern Greenland as viewed by the SSM/I at (a) 19 GHz and (b) 85 GHz. Red boxes mark (selected) grid-cells of the used polarstereographic grid. Ellipses denote the footprint area at the shown frequency. Ellipses and boxes are scaled relative to each other. Black (White) ellipses mark those footprints which overlap by at least (less than) 5% with the selected grid cells. Every other grid cell is shown at 85 GHz; at 19 GHz only three grid cells are shown for better visibility. The diagonal black and white lines denote the approximate distance from land up to which land surface brightness temperatures influence black and white footprints and thus the gridded brightness temperature. Note the scale bar at the lower right.

ice-extent differences are March/April (GS) and January (BS), and for the ice-area difference March/April (BS). These are all months with a high frequency of occurrence for cyclones. The large area-difference value for June in the GS, however, cannot be explained by this mechanism.

2.2.3. Correlation analysis. Correlation coefficients are calculated between the time-series of the monthly average sea-ice area anomaly of each calendar month, A_i, and the time-series of the monthly average sea-ice area anomaly of the successive months, A_{i+j}, according to the following equation:

$$R_{j,k} = CORR(A_i, A_{i+j,j=0\ldots j\max-k})_{k=0\ldots 11, i=1\ldots i\max.} \quad (1)$$

Index i counts the months of the time series for which k equals $i\,MOD\,12$, k denotes the calendar month, starting with January, and j denotes the time lag in months. The maximum time lag j used is $jmax = 48$ months for January and $jmax = 37$ months for December. The length of this lag was chosen such that the typical travel time of 1–3 yr (Pfirman et al., 1997; Kwok, 2009) of sea-ice exported out of the KS into the Arctic Ocean through gate III (Fig. 1) and later out of the Arctic Ocean into the GS and/or BS via gates I and II (Fig. 1) is covered. *MOD* stands for the mathematic Modulo operator, and $R_{j,k}$ is the correlation coefficient time-series obtained for the kth calendar month. When j equals 12, 24 or 36 the time-series used for the correlation computation are shortened by 1 yr.

Since this correlation analysis is not done with the area itself but with the area anomalies, instead of the Pearson correlation coefficient the Spearman rank correlation coefficient is used. The latter one is more robust in the presence of outliers (Jähne, 1997).

The significance of the obtained correlation coefficients is estimated with a permutation test (Sachs and Hedderich, 2006). By repeating the above calculation with a set of 10 000 randomly distributed ice-area anomalies A_{i+j} for each A_i an average random correlation coefficient is obtained (which is zero). Its standard deviation is subsequently taken as a measure of the significance levels, i.e. the obtained correlation coefficients are considered significant with a probability of more than 95% (99%) if their value exceeds the average random correlation coefficient plus two (three) times its standard deviation.

This analysis has been done to (i) identify auto-correlations of ice-cover anomalies within each region (intra-regional correlation), and to (ii) identify cross-correlations of ice-cover anomalies between the regions (interregional correlations). The results of this analysis have to be interpreted with great caution because even a significant correlation does not necessarily reflect a causal relationship. The discussion of the results of this analysis will focus therefore on those correlations that could be explained based on known ocean-ice-atmosphere feedback mechanism. Attention will also be paid to the memory of the ocean–ice–atmosphere system which certainly differs between the considered regions.

3. Results

3.1. Annual cycle

Figure 5 gives an overview about the average annual cycles of sea-ice extent and area for the entire period 1992–2008 (black) as well as subperiods 1992–1999 (blue) and 2000–2008 (red) for the five regions (Fig. 1). Regions IS, GS, and BS all show considerable changes in the annual cycle between 1992–1999 and 2000–2008. In region IS (Fig. 5a) the ice-free season increases from 1 month (Sep.) to 3 months (August–October). In region GS the timing of the average maximum sea ice extent and area has changed from Feb. during 1992–1999 to Mar. during 2000–2008 (Fig. 5b). Region BS tends to show a similar shift in the timing of the maximum sea-ice extent and area (Fig. 5c). Regions KS and WPS show least change during the two periods; region KS tends to be totally ice covered during December to May and has its minimum ice area and extent in September (Fig. 5d). In region WPS largest changes occurred in May/June and December (Fig. 5e). Table 1 summarizes the change in the average maximum and minimum ice-area and -extent values from 1992–1999 to 2000–2008.

3.2. Anomaly time series

Figure 6 shows time series of the average monthly sea-ice area and extent anomalies with respect to the average annual cycle of the ice area and extent during 1992–2008 (Fig. 5, thick black dotted and solid lines) for the period 1992–2008. Plots of the right-hand column additionally show the ice extent anomalies in relative units, which is the relative fraction of this anomaly compared to the average area. Tables 2 and 3 summarize the extreme values of the observed ice-area and extent anomalies, respectively.

In region IS (Figs. 6a–c) ice-area and -extent time series are dominated by negative anomalies in winters 2002/2003 and 2004/2005 and positive anomalies in winters 1992/1993 and 1994/1995. In region GS (Figs. 6d–f) large positive ice area and extent anomalies are associated with the presence of a pronounced Is-Odden (Latarius and Quadfasel, 2010): 1995/1996, 1996/1997, 1997/1998 and 2000/2001. Prior to 2001 negative anomalies occurred predominantly during the first half of the year but they were most prominent during summer later, i.e., in years 2002–2004 and 2006. In region BS (Figs. 6g–i) an almost uninterrupted prolonged period of negative ice-area and -extent anomalies is found starting in May 2004 and lasting until the end of our investigation period. The maximum negative anomaly occurred in May 2006. Largest positive BS anomalies occurred in May 1998. Positive BS anomalies have occurred more often during the first half of our observation period. In region KS (Figs. 6j–l) ice-area and -extent anomalies are observed predominantly during summer. The anomalies tend to switch sign every year during 1992–1998, and then every other

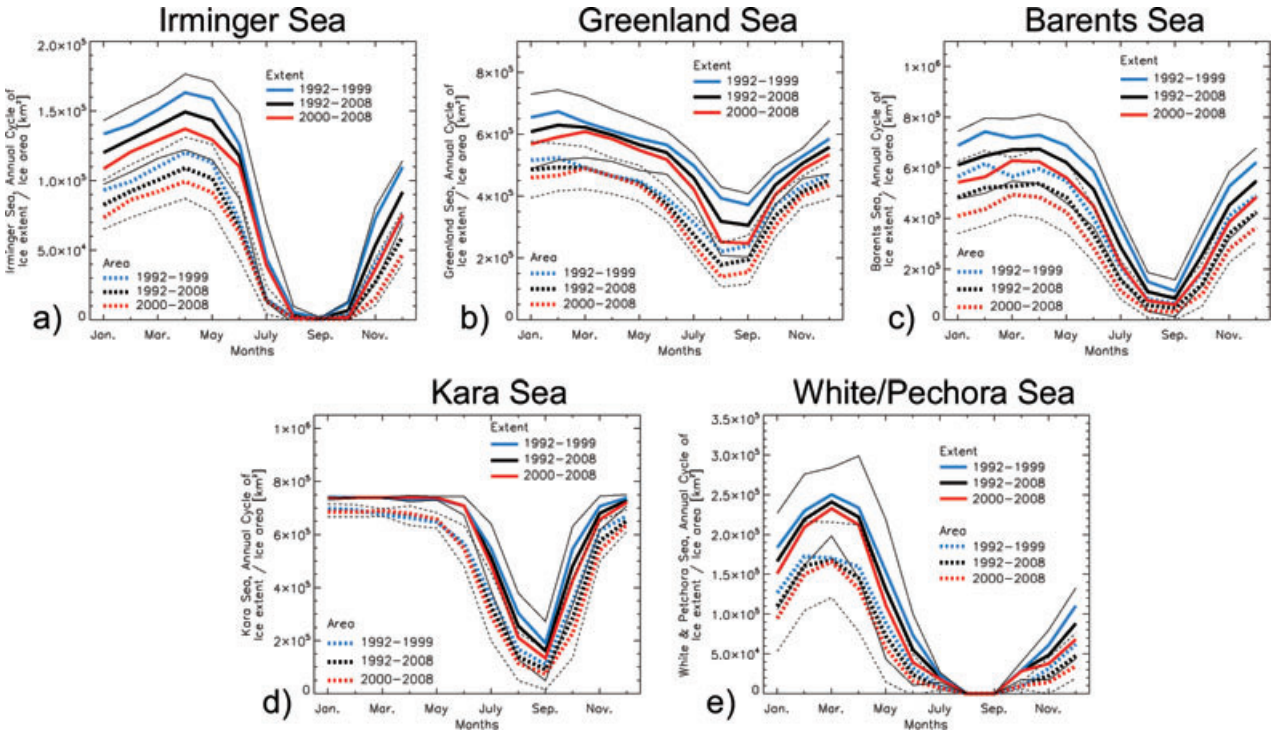

Fig. 5. Average annual cycles of the monthly average sea ice extent (solid lines) and area (dotted lines) for 1992–1999 (blue), 1992–2008 (black) and 2000–2008 (red) for (a) IS, (b) GS, (c) BS, (d) KS and (e) WPS. Thin solid or dotted black lines denote one standard deviation of the monthly average sea ice extent and area of 1992–2008.

Table 1. Change in the average maximum and minimum sea-ice area and extent (10^3 km^2) between 1992–1999 and 2000–2008

Season	IS	GS	BS	KS	WPS
Winter area	−20(−17%)	−37(−7%)	−121(−20%)	−2(−0%)	−18(−11%)
Extent	26(−16%)	−61(−9%)	−124(−17%)	−1(−0%)	−20(−8%)
Summer area	−0.5(−45%)	−83(−36%)	−40(−54%)	−44(−32%)	0
Extent	−2(−56%)	−133(−35%)	−65(−49%)	−74(−30%)	0

Notes: The maximum values are derived from a 3-month period centred at the month with the maximum ice area and extent (see Fig. 5); the minimum values are the average of the ice area and extent values of August and September. Values given in parentheses denote the change relative to 1992–1999.

year during 1998–2003. Since 2004 anomalies have remained mainly negative. Starting in 1998 annual average anomalies in the KS are in phase with those of region BS. In region WPS (Figs. 6m–o) ice-area and -extent time series are dominated by positive anomalies in winters 1997/1998 and 1998/1999. Although region WPS neighbours regions BS and KS observed WPS anomalies are not in phase with those of KS or BS. Note that relative positive (negative) ice-area and extent anomalies can exceed (may approach) 100% in all regions but GS (Fig. 6, Tables 2 and 3), and that these large relative anomalies did typically occur during/adjacent to summer months. The exception to this is region GS where the largest relative ice-extent anomaly occurred in winter 1996/1997 and was accompanied by a pronounced Is Odden.

We examined these anomalies with respect to a relationship to the monthly Arctic/North Atlantic Oscillation (AO/NAO) index (http://www.cpc.noaa.gov, see Fig. 6p). However, we found no clear relationship between the observed monthly ice-cover anomalies and the NAO- or the AO-index for any of the regions, and neither for the entire period (1992–2008) nor for the subperiods 1992–1999 and 2000–2008. Squared lag-correlation coefficients (not shown) computed between the time-series of the normalized (with respect to the absolute maximum value within 1992–2008) monthly NAO- or AO-index and monthly ice-area and -extent anomalies, using time lags in steps of one month between −12 and +12 months are all below 0.1 for 1992–2008 and thus not significant (95%-level: 0.26). The largest correlation coefficient ($R = -0.42$, $R^2 = 0.18$) is obtained

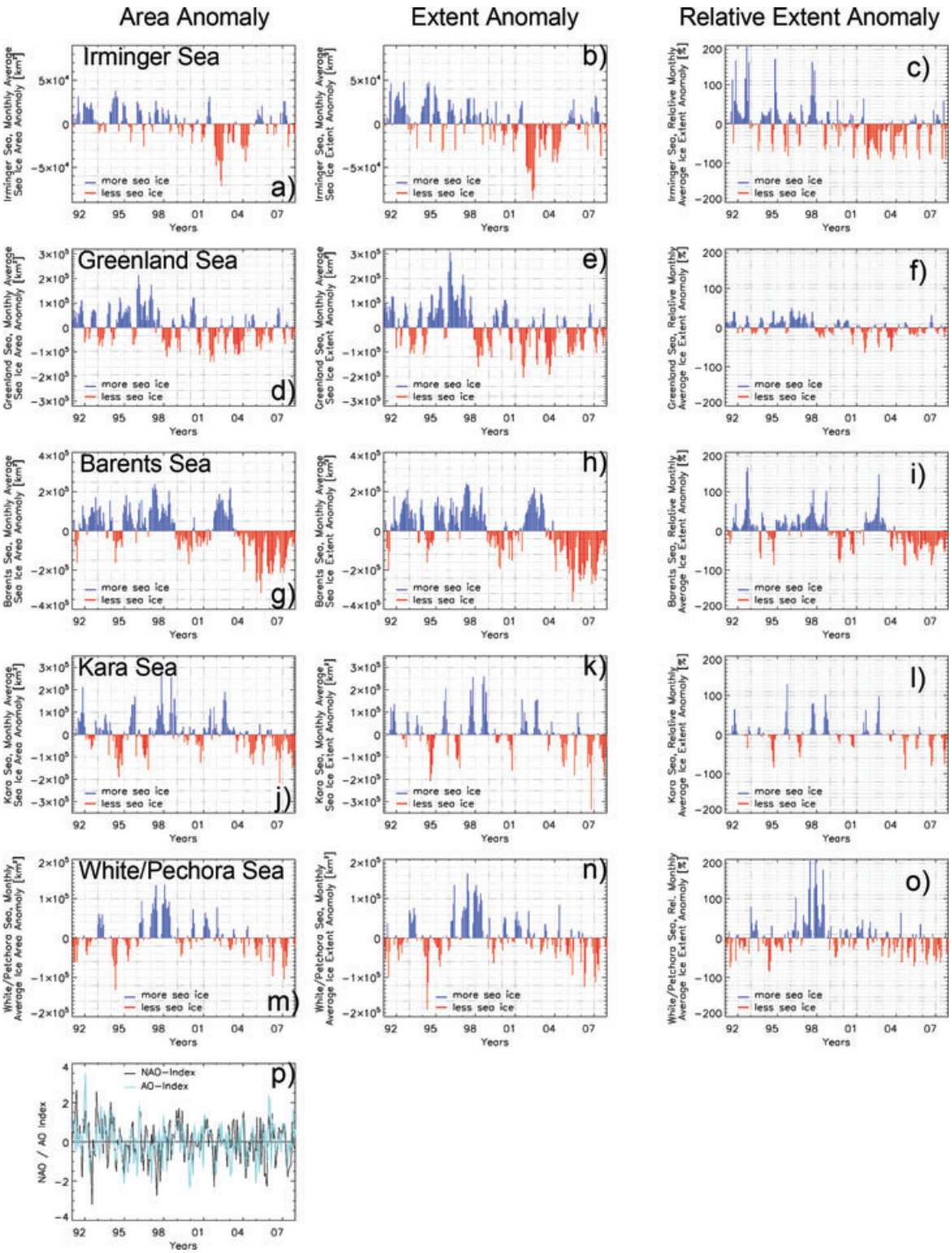

Fig. 6. Time series of the monthly average sea-ice area (left-hand column) and extent (middle column) anomaly relative to the average annual cycle for 1992–2008 (see Fig. 5) for (a, b) IS, (d, e) GS, (g, h) BS, (j, k) KS and (m, n) WPS. Note that negative (positive) anomalies are given in red (blue) in order to reflect the associated surface air temperature anomaly (warm = red, blue = cold). In addition the right-hand column denotes the monthly average sea-ice extent anomalies given in the middle column in relative units. Image (p) show the monthly NAO- and AO-Index taken from http://www.cpc.noaa.gov in black and cyan, respectively.

Table 2. Extreme ice-area anomaly during 1992–2008 (10^5 km^2) for each of the five study regions in absolute and relative units

	Minimum		Maximum	
	Absolute	Relative	Absolute	Relative
IS	−0.7(70%) (May 2003)	−93% (Nov. 2002)	+0.4(35%) (Apr. 1995)	>200% (Aug. 1993)
GS	−1.4(40%) (Oct. 2002)	−65% (Aug. 2002)	+2.1(44%) (Jan. 1997)	+69% (Aug. 1995)
BS	−3.7(64%) (May 2006)	−94% (Sep. 2005)	+2.4(36%) (Apr. 1998)	>200% (Sep. 1993)
KS	−2.2(86%) (Oct. 2007)	−92% (Sep. 2005)	+2.8(100%) (Oct. 1998)	+164% (Sep. 2003)
WPS	−1.3(90%) (Apr. 1995)	−92% (May 1995)	+1.4(124%) (Jan. 1999)	>200% (Jun./Nov. 1998)

Notes: The month and year of occurrence is given in parentheses and in general is different for the absolute and relative value. For the extreme months of the absolute ice area-anomalies additionally the relative ice-area anomalies are given in brackets.

Table 3. As Table 2 but for ice-extent anomalies

	Minimum		Maximum	
	Absolute	Relative	Absolute	Relative
IS	−0.9(60%) (May 2003)	−91% (Nov. 2002)	+0.5(116%) (Jul. 1993)	>200% (Aug. 1993)
GS	−2.1(64%) (Aug. 2002)	−64% (Aug. 2002)	+3.1(50%) (Jan. 1997)	+50% (Jan. 1995)
BS	−3.6(58%) (May 2006)	−89% (Sep. 2005)	+2.4(36%) (Apr. 1998)	+160% (Sep. 1993)
KS	−3.3(69%) (Oct. 2007)	−89% (Sep. 2005)	+2.6(104%) (Aug. 1999)	+129% (Sep. 1996)
WPS	−1.8(80%) (Apr. 1995)	−85% (May 1995)	+1.6(126%) (May 1998)	>200% (Jun./Nov. 1998)

between the NAO-index and GS ice-area anomalies of 1992–1999 and a time lag of 1 month. The respective correlation coefficient (same time lag, same period) with the AO-index is $R = -0.31$ ($R^2 = 0.1$). Both correlation coefficients are not significant (95%-level: 0.35), though. Note that Kwok (2009) and Vinje (2001) reported that particularly during the negative phase of both the AO and NAO the relationship between Fram Strait ice-area export and these indices is less robust. As we will see later, GS and IS ice-area and extent anomalies are related to Fram Strait ice-area fluxes, so that the observed lack of correlation found in this paper seems reasonable.

3.3. Intra-regional correlations

Figure 7 shows the autocorrelation between ice-area and -extent anomaly time-series of 1 month for 1992–2008 (called reference time series henceforth) and the corresponding anomaly time-series of following months for at least three annual cycles. Only correlation coefficients with 95% significance level are shown; those with 99% significance are surrounded by black boxes. In region IS (Figs. 7a and b) significant correlations are basically limited to the next 1–2 months from October to June. November to February ice anomalies are correlated to ice anomalies of a longer period: 3–5 months. Note that extent anomalies have on average a 1 month longer significant correlation. In region GS (Figs. 8c and d) ice-area and -extent anomalies of months December to February and of June (extent: April) to September are correlated to respective anomalies of the next 2–3 months. In other months correlations are either not significant or only with the next month, as for March or November. Correlations between BS ice-area and -extent anomalies (Figs. 8e and f) confirm the quasi-periodic nature of these anomalies evident from Figs. 6g–i). Correlations can last for up to 15 consecutive months. Ice anomalies of months September and October show least correlation with ice anomalies of the subsequent months. In region KS (Figs. 7g and h) significant correlations are limited to the summer period with a maximum auto-correlation duration between 2 and 5 months for May (extent: June) to September. During winter correlations are practically absent because of the almost complete coverage of region KS with sea ice. WPS (Figs. 7i and j) ice-area and -extent anomalies show significant correlations particularly during winter with a duration between 3 and 5 months from January to March. Ice-concentration anomaly maps shown in Figs. 7k–n) exemplify the anomaly distribution for years 2003 and 2006, giving an example for positive (k and l) and negative (m and n) anomalies in months January and June that contribute to, for example, the autocorrelation observed for region BS. Note that regions IS and GS show some significant autocorrelations particularly between ice-extent anomalies also for longer time lags (Figs. 7b and d); these will not be examined further in this paper, however.

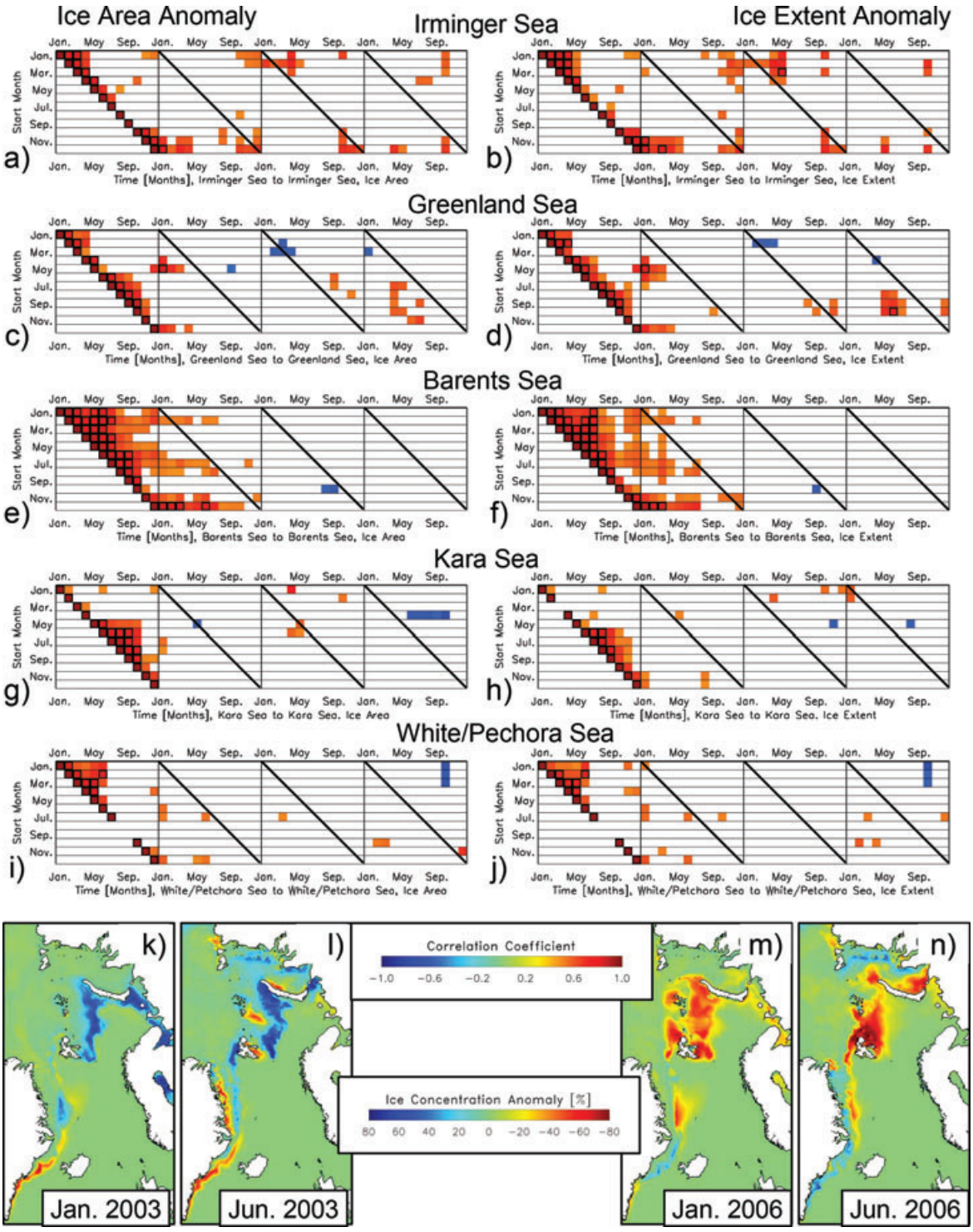

Fig. 7. Spearman Rank correlation coefficients *R* between the sea-ice area (left-hand panel) and extent (right-hand panel) anomaly time series of each calendar month (*y*-axis) during 1992–2008 and the sea-ice area and extent anomaly of the succeeding months for at least three full annual cycles (*x*-axis) for each region of interest (Fig. 1). Shown is the autocorrelation with the sea-ice area and extent anomalies of the same region (different to Figs. 8–11). Minimum time lag is zero, maximum time lag is 47 months for January and 36 months for December. The correlation coefficients are colour coded according to the given legend. Only *R*-values which are significant at a significance level of 95% or higher are shown; those at a significance level of 99% are additionally marked by black boxes. Images (k)–(n) show examples of a pair of positive and negative ice-concentration anomalies of the indicated months to underline the observed autocorrelation in region BS (e, f).

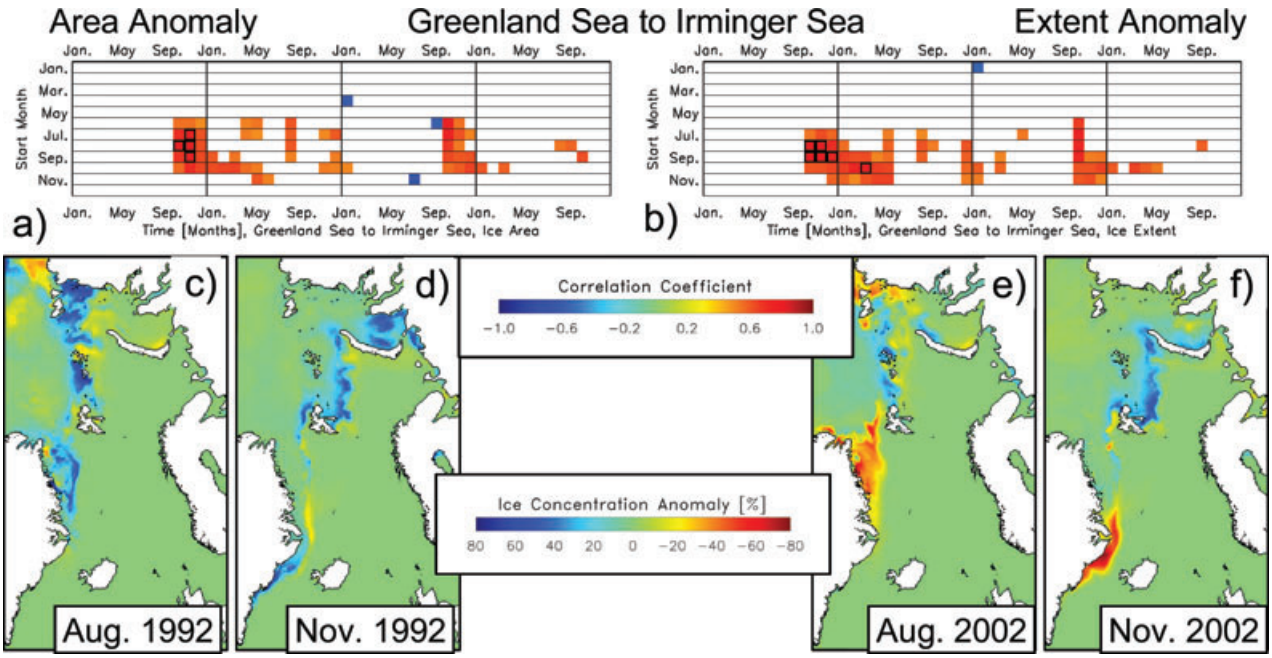

Fig. 8. As Fig. 7 but for the correlation of sea-ice area (a) and extent (b) anomalies of region GS with those of region IS. Images (c) to (f) show examples of a pair of positive and negative ice-concentration anomalies of the months indicated.

3.4. Inter-regional correlations

Figures 8–11 are similar to Fig. 7 except that the reference time series is taken from a different region as the time-series of the following months; in other words: these figures show cross-correlations. June to October (extent: July to November) GS ice-area and -extent anomalies shown in Figs. 8a and b) are correlated to respective IS ice anomalies during the following freezing season. While for ice area the correlation is confined basically to the period October to December, except October where the correlation lasts for Oct. to May (Fig. 8a), for ice extent the correlation in general lasts longer, particularly for September and November. Figures 8c–f exemplify this correlation for a positive (c and d) and a negative (e and f) pair of anomalies. Interestingly, no significant correlation exists between winter GS ice-area and -extent anomalies and respective IS ice anomalies. Note that a second period of significant but smaller correlations is shown for almost the same months for the next but 1 yr.

Figures 9a and b show the correlation between BS and KS ice-area and extent anomalies. A significant correlation is evident between both regions in September/October. This is illustrated by images c–f in Fig. 9 showing examples of positive (c and d) and negative (e and f) ice-concentration anomalies in both regions in the same month (October). December to March BS ice-area and -extent anomalies are correlated with respective KS ice anomalies in July to September/October/November (extent: August to September/October). This is illustrated by images g–j) in Fig. 9 showing examples of positive (g and h) and negative (i and j) ice-concentration anomalies in region BS in January/February and region KS the subsequent July. Finally, BS ice-area anomalies of months June to August are correlated with KS ice-area anomalies from July/August to November. Note that for ice-extent anomalies correlations are smaller and durations are shorter compared to ice-area anomalies.

Figure 10 shows the correlation between BS and WPS ice-area and extent anomalies (images a and b) and between WPS and KS ice-area and -extent anomalies (images c and d). BS ice-area and -extent anomalies of months February to May are correlated with respective anomalies in region WPS for May/June. Significant correlations are also evident between October/November/December BS ice-cover anomalies and those in region WPS 1 month later. WPS ice-area and -extent anomalies during January are correlated with KS ice-area and extent anomalies during the same month but more pronounced during the entire period May to January (extent: June to November). This is illustrated for months January, June and July in images (e)–(j) of Fig. 10 showing positive (e–g) and negative (h–j) ice-concentration anomalies. Correlations between ice-area and -extent anomalies of the same month occur also for November and December.

Finally, correlations between GS and BS ice-area and extent anomalies are shown in Figs. 11a and b, respectively. January to May (extent: June) GS ice-area and—extent anomalies are correlated to respective BS ice-cover anomalies with a time lag of between 12 and 24 months and a duration of between 1 (March) and 12 (January) months (Figs. 11a and b). Largest correlations occur between January GS and June BS ice-area and -extent anomalies and between those of February (GS) and

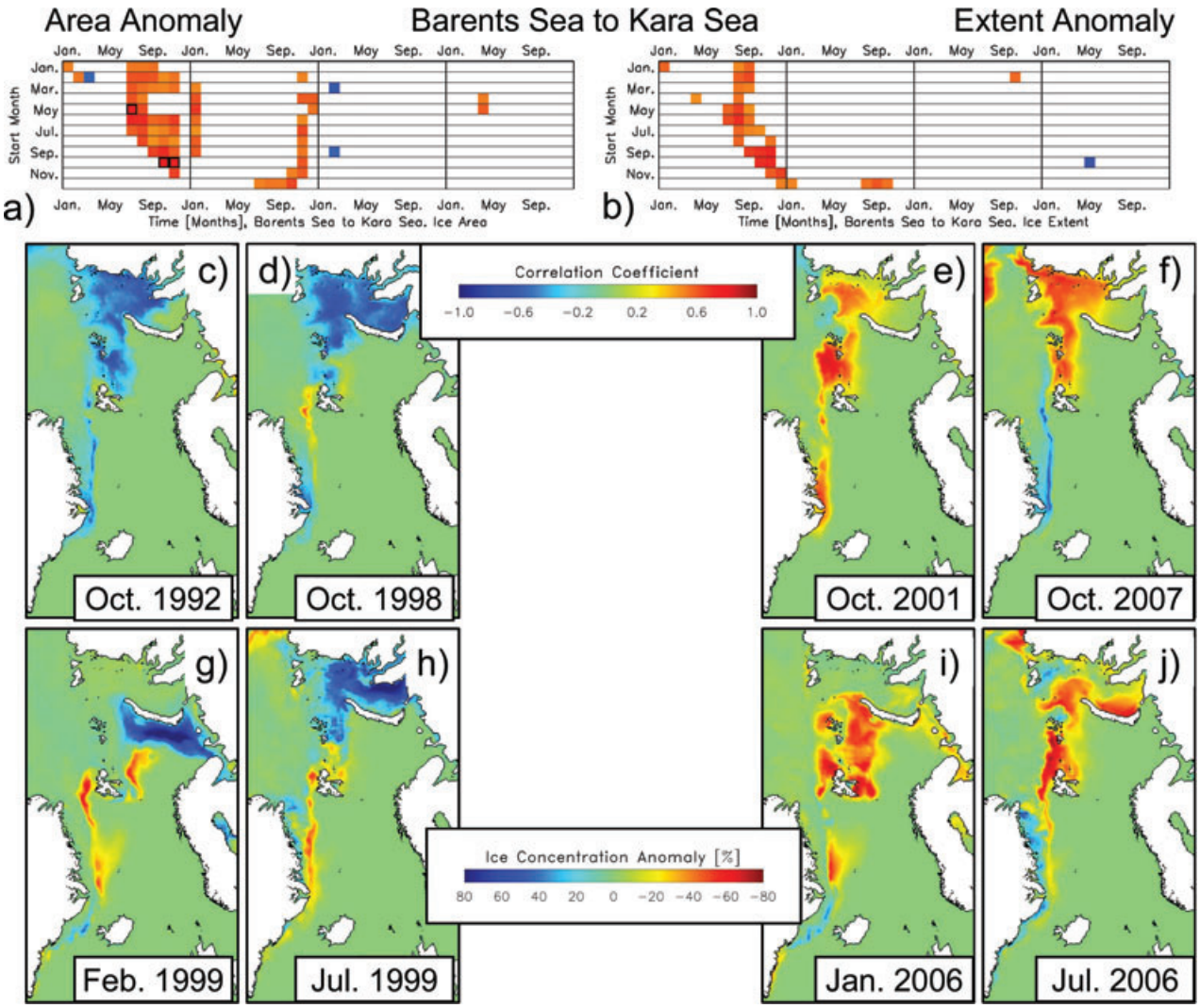

Fig. 9. As Fig. 8 but for the correlation of sea-ice area (a) and extent (b) anomalies of region BS with those of region KS. Images (c) to (f) show examples of positive and negative ice-concentration anomalies for October to underline the observed spatial coexistence of anomalies. Images (g) to (j) show examples of a pair of positive and negative ice-concentration anomalies of the months indicated.

October (BS). Examples for the associated ice-concentration anomaly distributions are given in Figs. 11c–f.

4. Interpretation and discussion

4.1. Regional characteristics

We consider the period 1992–2008 and observe changes in the annual cycle of the average monthly ice extent and area between periods 1992–1999 and 2000–2008 in all ROIs (Fig. 5, Table 1) with different characteristics. In regions IS, GS and BS changes are evident for almost the entire annual cycle: maximum (minimum) ice area and extent decreased by 17, 8 and 18% (50, 35 and 51%), respectively. WPS minimum ice area and extent did not change since it is already zero, while maximum ice area and extent decreased by about 10%. Maximum KS ice area and extent values remain unchanged, while minimum ice area and extent values decreased by about 31%. These changes are smaller than the numbers found by Rodrigues (2006, 2008) for summer and winter ice-area and extent changes for the period 1979–2006. This is partly caused by the different reference period: 1979–2006 against 1992–2008. Furthermore, Rodrigues (2006, 2008) examined changes in the mean winter and summer ice-area and extent while mean maximum and minimum values are considered in this paper.

We also observe a larger number of negative ice-area and extent anomalies in regions GS, BS and KS after 2001, 2003 and 2004, respectively (Fig. 6). Moreover, according to Fig. 6 ice-area and -extent anomalies typically occur only over an uninterrupted period of a few subsequent months in all but region

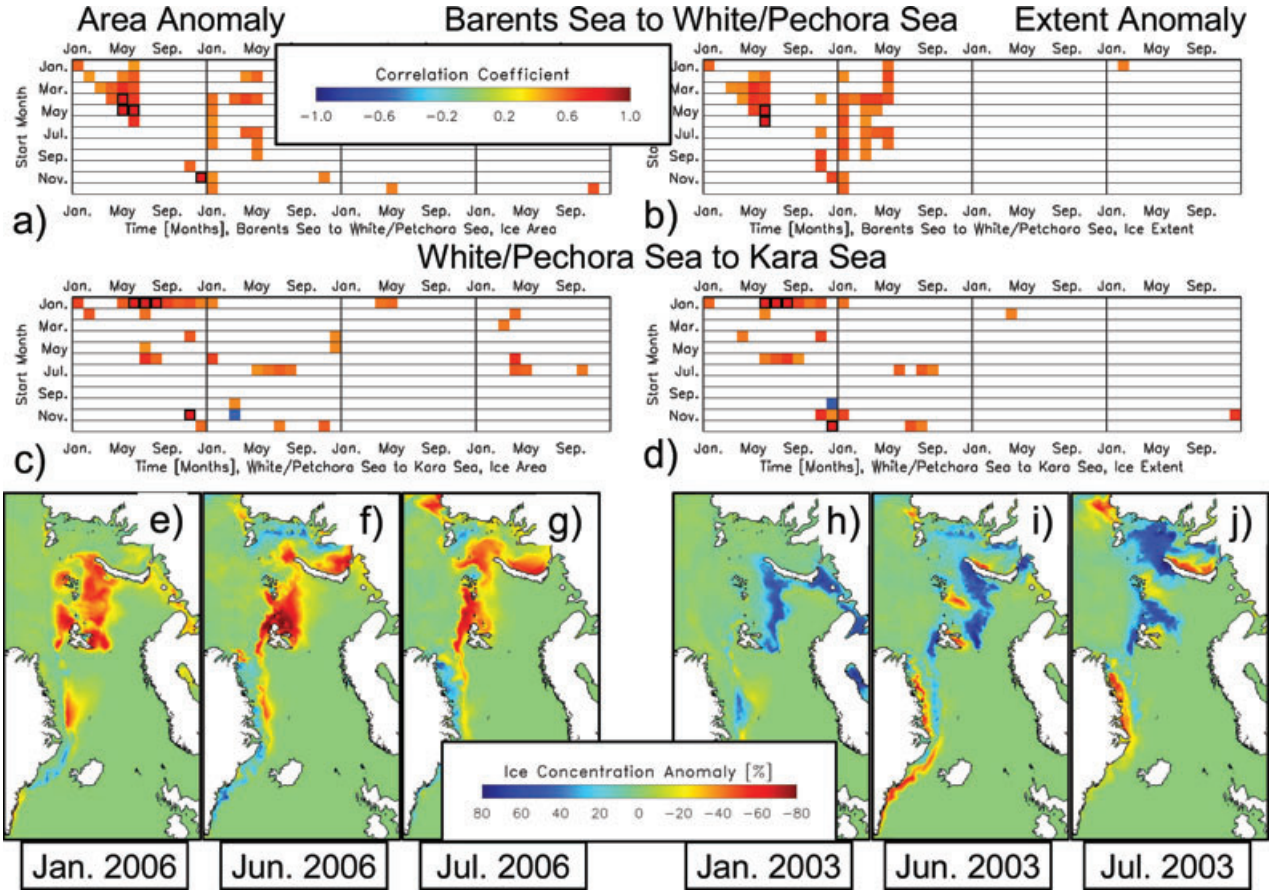

Fig. 10. As Fig. 8 but for the correlation of sea-ice area (a, c) and extent (b, d) anomalies of regions BS and WPS with those of regions WPS (a, b) and KS (c, d), respectively. Images (e) to (j) show examples of a triplet of positive and negative ice-concentration anomalies of the months indicated.

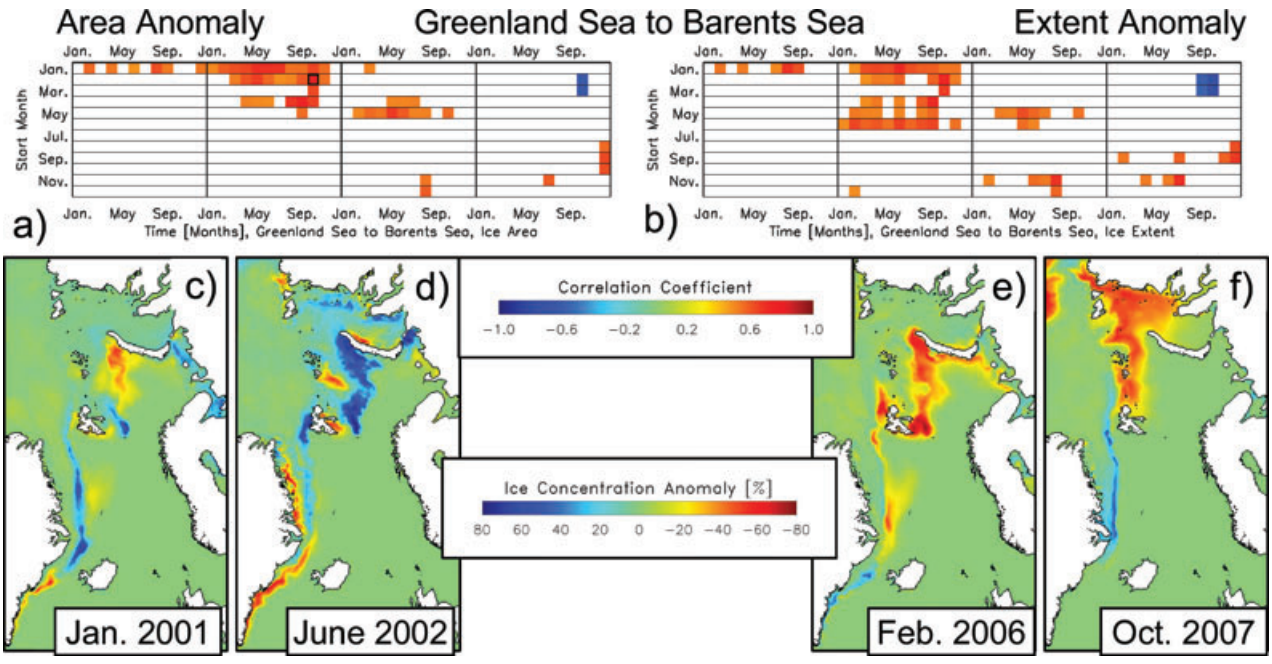

Fig. 11. As Fig. 8 but for the correlation of sea-ice area (a) and extent (b) anomalies of region GS with those of region BS.

BS; exceptions are years with an extreme Is Odden 1996, 1997 (GS), the positive ice-cover anomaly in region WPS in years 1998/1999, and the negative ice-cover anomaly in region IS in years 2002–2004. In contrast BS ice-area and -extent anomalies typically last over a longer uninterrupted period of subsequent months. Note that extreme large ice area and extent values occurred during 1992–1999 while the extreme small ones occurred during 2000–2008 (Tables 2 and 3).

The auto-correlation matrices of regions IS and GS indicate a rather short duration of the auto-correlation of 2–3 months (Figs. 7a–d). The same is true on average for regions KS and WPS (Figs. 7g–j); however, here not all months can be considered for the discussion because region KS is almost totally ice covered from December to May and region WPS is almost totally ice free from July to Oct. Autocorrelation matrices for region BS (Figs. 7e and f) indicate an average duration of the autocorrelation of 6–7 months, that is, twice as long as observed for the other regions.

For IS and GS this can be explained as follows: most of the sea ice in region GS is imported via Fram Strait out of the Arctic Ocean. The majority of it drifts southward driven by the East Greenland Current (EGC) and the predominant northerly surface winds. Consequently, any ice-cover anomaly is transported south and only during episodes of a weaker EGC or weaker surface winds (as for example in region GS during summer) this transport slows down and ice-cover anomalies can stay longer. The same is true for region IS, except that it receives most of its ice via Denmark Strait (see Section 4.2), and that local ice formation plays an even smaller role in region IS than in region GS, where positive anomalies in ice area and extent could be caused by enhanced ice import via Fram Strait but also by extensive local ice formation as associated with an Is Odden event (Shuchman et al., 1998; Comiso et al., 2001). Shuchman et al. (1998) investigated the period 1978/1979 to 1994/1995 and identified, for instance, the local surface air temperature followed by the local surface wind speed as the main drivers for the development of an Is Odden, while Rogers and Hung (2008) identified the general atmospheric circulation NAO- pattern as the main driver on the large-scale.

In region KS significant auto-correlations start in May/June, that is, at melt onset, and end in October/November, that is, at freeze-up. The development of KS ice area and extent during summer and fall months is sensitive to the occurrence of an ice-area and -extent anomaly in any preceding month starting in May/June. Negative (positive) ice-cover anomalies in June are likely followed by negative (positive) ice-cover anomalies in July/August; negative (positive) ice-cover anomalies in Aug. are likely followed by negative (positive) ice-cover anomalies in September/October.

In region WPS significant autocorrelations between ice-area and -extent anomalies of between 2 and 5 months duration are observed only for December to May (Figs. 7i and j); they are most pronounced from January to March, that is, the main freezing season in this region. It could be argued that the ice cover in these months preconditions the ice cover until complete melt off in June. However, since region WPS could be considered as part of region BS it can be expected that the same feedback mechanisms (see below) apply to region WPS as well, except ice import out of the Arctic Ocean.

The duration of autocorrelations in region BS (Figs. 7e and f) is twice as long as in the other four regions. Several explanations can be given for this behaviour. The first one is a local ocean–ice–atmosphere feedback mechanism. A positive ice-cover anomaly at the end of winter is associated with a negative surface air-temperature anomaly. Both, more ice and lower temperatures, reduce the energy flux from the atmosphere to the open water area in the BS. This delays melt onset causing a positive ice-cover anomaly in subsequent months. In addition, associated with positive ice-cover anomalies during winter is a positive ice-thickness anomaly which also delays sea-ice melt in region BS. Further, a positive ice-cover anomaly during summer (June/July) is associated with a negative surface air-temperature anomaly, and with less heating of the surface water layers. This may cause an earlier freeze-up in region BS in the subsequent fall/winter. The opposite is true if starting with a negative ice-cover anomaly at the end of winter. An important aspect in this context is the fact that if the summer ice melt water anomalies are not carried away by surface currents, as is the case in regions GS and IS, they can enhance or reduce the upper water layer stratification, thereby reduce or enhance vertical oceanic heat flux and this way precondition the surface water layer for earlier or delayed ice formation in the subsequent fall.

The second one is a feedback between BS and the Arctic Ocean via ice export through gates II and III (see Fig. 1) which we will discuss later. Note however, that a substantial import (export) of sea ice into (out of) region BS could both enhance and reduce the effects produced by the above-mentioned local feedback mechanism.

The third one is the large-scale forcing by ocean and atmosphere independent of the BS ice cover. The northward advection of a positive (negative) oceanic heat anomaly from the northern North Atlantic into the BS is associated with a typical NAO+ (NAO−) situation, which causes a northward shift and strengthening (southward shift and weakening) of low-pressure systems entering the BS. The immediate effect is the northward (southward) transport of warmer (colder) air masses with more (less) on-ice air flow, a northward retreat (southward extension) of the sea-ice edge, and a positive (negative) sea surface temperature (SST) anomaly (Francis and Hunter, 2007; Deser and Teng, 2008). Associated with this shift in cyclone activity the inflow of Atlantic water into the Nordic Seas and further into region BS is modulated, causing oceanic heat anomalies to arrive in region BS with 1–2 yr time lag (Dickson et al., 2000; Sorteberg and Kvingedal, 2006). These anomalies may cause a continuation or even enhancement of the positive BS SST and negative ice-extent anomalies by, for example, enhanced

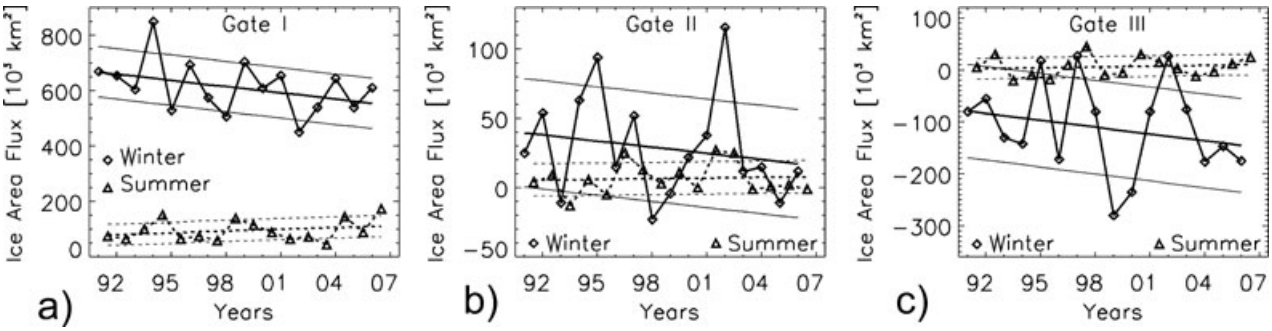

Fig. 12. Sea-ice area flux for winter (Oct.–May) and summer (June–September), 1991/1992–2006/2007 through gate I (a), gate II (b) and gate III (c) (see Fig. 1) as taken from Kwok (2009). Superimposed are trends (thick lines) based on a linear regression fit for winter (solid) and summer (dotted) together with the range given by the RMSE between fit and data (thin lines).

ocean-atmosphere heat transfer and continued cyclone activity. Or the effect these anomalies can have, could be balanced by enhanced ice import into region BS by, for example, a changed atmospheric circulation pattern, causing increased stratification of the surface water layers by melt water and thus inhibit enhanced ocean–atmosphere heat transport (Gerdes et al., 2003; Bengtsson et al., 2004; Sorteberg and Kvingedal, 2006). Since this latter mechanism is driven mainly by the oceanic heat content which varies more slowly compared to the ice and atmosphere, it is likely that its effect on the ice cover is visible over a period of several months to a few years—as we observe in BS ice-area and extent anomalies (Figs. 6g–i) and their correlations (Figs. 7e and f). Recently, Zhang et al. (2008) reported a northeastward shift of the location of the centres of action of the AO/NAO during the pentad 2001/2002–2005/2006. According to Zhang et al. (2008) this shift favours enhanced heat input into region BS in concert with southerly/westerly winds and a northward retreat of BS ice cover over a period of a few years.

Feedbacks between regions GS and KS with the Arctic Ocean via ice export through gates I and III (Fig. 1) will be discussed later. Note that large-scale atmospheric forcing is known to set the boundary conditions for all regions (Kwok et al., 2004; Francis and Hunter, 2007; Deser and Teng, 2008; Rogers and Hung, 2008), while an influence of oceanic heat anomalies like described for region BS is less likely for the other regions. We surmise that in region WPS the inflow of an oceanic heat anomaly (Atlantic water) is less frequent, because the main flow through the Barents Sea occurs north of region WPS (Maslowski et al., 2004). Region KS can be affected by such ocean heat anomalies by their transport around the northern tip of Novaya Zemlya trough the northwestern-most part of region KS before it exits this region via St. Anna Trough, and by transport through the Kara Gate (Maslowski et al., 2004). Note that the transport through the Kara Gate amounts roughly 1/10 of the inflow between Svalbard and Norway. In regions GS and IS Atlantic water heat anomalies are recirculating and steered southward by the topography. On the shelf the cold and comparably fresh water exiting the Arctic Ocean inhibits ocean-atmosphere heat transfer, which can be altered by a ocean heat anomaly. Off the shelf the influence of oceanic heat anomalies onto the ocean–atmosphere heat transfer becomes more likely and might, for example, hamper the formation of an Is Odden (Visbeck et al., 1995).

4.2. Interaction GS–IS

Correlation matrices shown in Fig. 8 indicate that GS and IS ice-area and extent anomalies are correlated with each other. We explain this with the fact that the IS ice cover is dominated by ice import out of region GS via Denmark Strait. Images c–f) of Fig. 8 demonstrate how the location of a positive (c and d) or negative (e and f) ice-concentration anomaly changes over time from August to November.

Region GS receives much of its ice cover via ice import through Fram Strait (Fig. 1, gate I, see Fig. 12). While during winter local ice formation might mimic variations in the amount and thickness of ice imported into GS via Fram Strait there is no compensating effect during summer. We surmise therefore that if region GS receives less sea ice via Fram Strait a negative ice-area and -extent anomaly will develop and vice versa, that is, that ice-flux anomalies through Fram Strait are correlated with GS ice-area and -extent anomalies, provided that the general atmospheric and oceanic situation remains rather constant. We surmise further, that because of the above-mentioned correlation between GS and IS ice-cover anomalies, a correlation between ice-flux anomalies through Fram Strait and IS ice-area and -extent anomalies can be observed also.

Winter (Oct.-May) and summer (June–September) ice-area flux estimates through Fram Strait given by Kwok (2009) for the period 1991/1992–2006/2007 are displayed in Fig. 12a) together with their trends (see Table 4). The obtained ice-area flux anomalies are compared to IS and GS ice-area and -extent anomalies for the same periods (IS: winter: December–June, summer: July–November) by means of a lag-correlation. The results are given in Table 5 and indicate, that winter ice-area flux anomalies are positively and significantly correlated to GS summer ice-area and -extent anomalies but not to the winter

Table 4. Trends in the winter (October–May) and summer (June–September) ice-area fluxes in km^2 per year through gates I, II and III as displayed in Fig. 12

Season	Gate I	Gate II	Gate III
Winter	-7600 ± 5200 (-1.2%)	-1500 ± 2100 (-5.3%)	-4400 ± 4900 (-5.0%)
Summer	$+2100 \pm 2100$ ($+2.1\%$)	$+200 \pm 600$ ($+2.4\%$)	$+500 \pm 1000$ ($+10.8\%$)

Note: Values given in parentheses denote the given trend as percentage of the mean ice-area flux for the period 1991/2002–2006/2007. Note that trend values have been rounded to the nearest 100 km^2.

Table 5. Results of a lag correlation between winter (October–May) and summer (June–September) ice-area fluxes through gate I (Fig. 1) taken from Kwok (2009) for 1991/1992–2006/2007 (see Fig. 12) and IS and GS ice-area and -extent anomalies

	Irminger Sea	Greenland Sea
Season	Area, Extent	Area, Extent
S2S	–,–	–,–
S2W	–,–	–, −0.51
W2W	**0.55**, **0.56**	–,–
W2S	0.51, **0.52**	**0.56**, **0.57**

Notes: Given is the correlation coefficient R with a minimum significance level (S-level) of 90% (based on a permutation test with 10 000 members). Values for area and extent are separated by a comma. Acronyms S2S, S2W, W2W and W2S stand for correlations of data between summer, summer and winter, winter, and winter and summer, respectively. Correlations with a S-level of 95% or more are highlighted bold. Note that summer (winter) is July–November (December–June) in region IS, while it is June–September (October–May) for region GS. The time lag is always zero years.

ones; correlation coefficients are small, however. This agrees with the above said: variations in winter GS ice-area and extent during 1992–2007 cannot be explained with variations in winter ice-area import because of the varying local ice formation, while variations in summer GS ice-area and extent during 1992–2007 are linked to variations in ice-area import during the preceding winter. It is likely that the correlation would increase if we would take ice-area flux values of months Mar.-May and correlate them with the summer ice-area and -extent anomalies because of the relatively short duration of the autocorrelation of ice-cover anomalies in region GS (Figs. 7c and d). Table 5 indicates that winter Fram Strait ice-area flux anomalies are correlated with winter (the same one) and summer (the subsequent one) IS ice-area and -extent anomalies. So in contrast to region GS variations in winter ice-area flux through Fram Strait can cause variations in winter and summer IS ice-area and extent. If we assume a typical ice-drift speed of 10 km d^{-1} the average travel time from Fram- to Denmark Strait is about 3–4 months. If we further take into account that (see above) for IS we defined winter as the period December–June) the high winter to winter correlation with no time lag seems to be reasonable.

The winter (summer) ice-area flux through Fram Strait shows a negative (positive) trend, which is significant at 68% significance level (Fig. 12a, Table 4). The reasons for such a negative trend could be (i) a decrease in ice concentration, and/or (ii) a decrease in ice drift speed. According to Kwok (2009) the former seems to be the case also if we consider the shorter period 1992–2008 of this study. Kwok (2009) show an approximately 2% per decade decrease of the 1992–2008 winter mean-ice concentration across Fram Strait. This cannot be confirmed by Fig. 13, which shows profiles of the mean annual, summer (June–September), and winter (October–May) ASI ice concentration across Fram Strait. These profiles exhibit quite some variability of the mean ice concentration, particularly along the eastern part of the transect, but a systematic shift towards a smaller ice concentration cannot be identified in this figure. Concerning (ii) Rampal et al. (2009) found an increase in the sea-ice mean drift speed along the Greenland coast by 1 km d^{-1} (from 9 to 10 km d^{-1}) during winters 1992–2004, and Kwok (2009) reported a (weak) increase of the across-strait mean surface pressure gradient for (1992–2007) 1979–2007, which also causes an increase in the sea-ice mean drift speed. However, if we, for simplicity assume a constant mean ice concentration value across the Fram Strait of 80% and a constant mean ice drift speed of 9 km d^{-1} and apply the above-mentioned changes the resulting ice-area export would increase from 1992 to 2007. This contradicts Figure 12a and Table 4, and thus Kwok (2009). We conclude that the temporal variability of the across Fram Strait ice-concentration (see also Fig. 13) and ice-drift speed distribution is too large, and the involved time series are too short to use the above-mentioned changes in these quantities to further evaluate or interpret the ice-area flux trend. It cannot be ruled out however, that because of the indicated relationship between winter Fram Strait ice-area flux and GS as well as IS ice-cover anomalies (Table 5) the observed decrease in ice-area flux (Fig. 12a) partly explains the reduction in GS and BS ice covers shown in Fig. 5 and Table 1.

Another aspect is the ice thickness. A thickness decrease of sea ice entering region GS via Fram Strait would explain a decrease in GS ice-area and extent during late spring/summer because the sea ice melts away faster; in fact the ice-area and extent reduction in region GS is largest in summer (Fig. 5b, Table 1). At the same time less sea ice would arrive at Denmark Strait and would thus be imported into region IS; the consequence

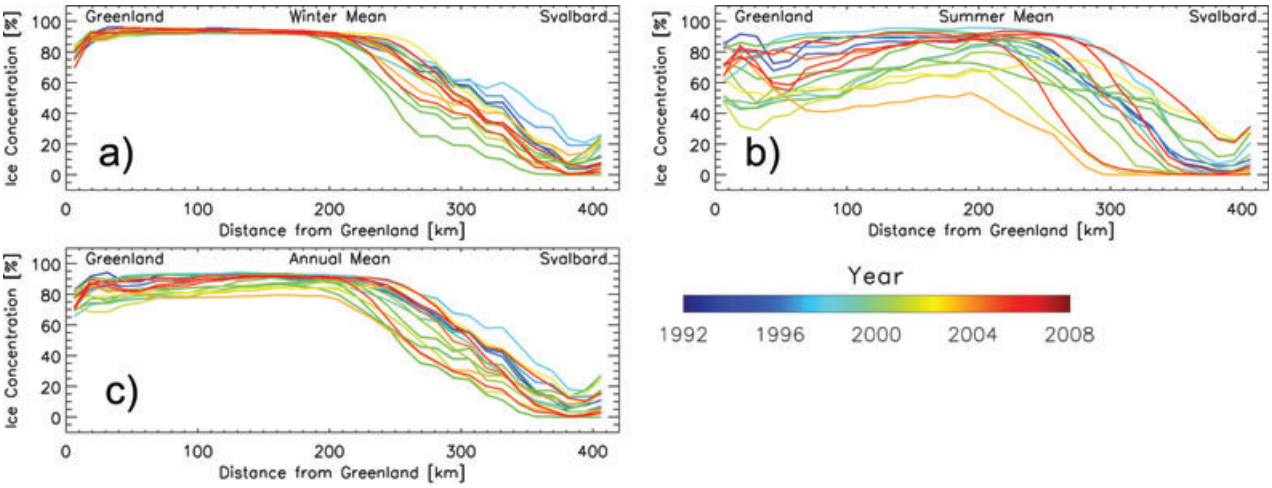

Fig. 13. Profiles of the mean winter (October–May, a) summer (June–October, b) and annual (c) ASI algorithm ice concentration across the Fram Strait along gate 1 (see Fig. 1) for 1992–2008. Each line represents 1 yr according to the colour legend.

would be a reduction of the IS ice cover as well as an increase of the ice-free season as observed in this study (Fig. 5a) and as found by Rodrigues (2009). However, the ice-volume flux through Fram Strait during 2003–2008 seems not to differ from the one during the 1990s (Spreen et al., 2009). At the same time the winter ice-area flux has remained rather constant for 1979–2007 as did the annual ice-area flux (Kwok, 2009). Since summer and winter ice-area flux trends have opposite signs for 1992–2007 (Fig. 12a, Table 4) the ice-area flux through Fram Strait derived for the present study can also be assumed constant for 1992–2007. However, if neither the ice area flux nor the ice-volume flux has changed, the ice thickness has remained constant as well, which is confirmed by Kwok and Rothrock (2009) by comparing ice-thickness observations in the Nansen Basin adjacent to the Fram Strait of 1993–1997 and 2003–2007. The above-mentioned reductions in GS and IS ice-area and -extent therefore cannot be explained with the current knowledge of the sea-ice area and volume import out of the Arctic Ocean.

Is Odden events occurred in winters 1995/1996 to 1997/1998 and 2000/2001 covering a total area of approximately (110, 215, 180 and 130) $\times 10^3$ km^2, respectively (Latarius and Quadfasel, 2010). These areas account for between 24 and 46% of the average 1992–2008 GS ice area in months January–May (460 $\times$ 10^3 km^2). Three of these events occurred during 1992–1999, only one during 2000–2008. If we assume that these events are the primary source for larger GS ice-area and -extent anomalies and if we distribute their (cumulative) area equally over the two periods 1992–1999 and 2000–2008 we obtain a surplus of 63 000 km^2 for 1992–1999 and of 14 000 km^2 for 2000–2008. The difference: 49 000 km^2 is of the order of the observed ice-area reduction (Table 1). We conclude therefore that the lack of Is Odden events and the associated westward retreat of the GS ice cover during 2000–2008 compared to 1992–1999 could be one reason for the observed winter GS ice area and extent decrease.

4.3. *Interaction BS–KS*

Figures 6g–i indicate that BS ice-area and -extent anomalies of the same sign typically last much longer than in the other four regions; one can speak of 1–2 yr long episodes of positive or negative anomalies. This is confirmed by the long duration of autocorrelations of BS ice-area and -extent anomalies shown in Figs. 7e and f). While positive anomalies dominate period 1992–1999 negative ones dominate period 2000–2008. Starting in 1998 KS ice-area and -extent anomalies start to be in phase with those observed in region BS (see Figs. 6j–l).

We found that fall (September to November) BS ice-area and -extent anomalies coincide with KS ice-cover anomalies during September to November (December) (Figs. 9a and b). If sea ice remains in either of these two regions at the end of summer it is likely that it is present in the other region as well because they neighbour each other (see also Figs. 9c–f). We also identified a relationship between BS ice-area and -extent anomalies during practically the entire first half of the year (January to July) with KS ice-area and -extent anomalies from July to September (see also Figs. 9g–j).

In Section 4.1, we have identified four major reasons for the autocorrelation pattern in region BS: local ocean-ice-atmosphere feedback, feedback with the Arctic Ocean via ice im-/export, the general atmospheric circulation, and oceanic heat transport anomalies. We have further pointed out that the latter reason is far less important for regions KS and WPS than for region BS. Based upon this we surmise that the above-mentioned ice-area and -extent anomaly coincidence and correlation between regions BS and KS is caused by a feedback between the effects

of the general atmospheric circulation in these regions and the local ocean–ice–atmosphere interaction mechanism (Bengtsson et al., 2004; Sorteberg and Kvingedal, 2006). The typically associated atmospheric surface air pressure pattern supports the advection of cold continental air in case of a positive BS ice-cover anomaly, or of mild maritime air in the opposite case; the former supports, the latter hampers thermodynamic sea-ice growth in the BS and also the KS. Consequently, positive (negative) wintertime BS ice-cover anomalies can be responsible for a thicker (thinner) KS ice cover at the end of winter, which needs more (less) time to melt. Positive oceanic heat anomalies in region BS as time-lagged result from enhanced cyclonic activity in the Nordic Seas and BS can bias this relationship towards a more pronounced positive feedback mechanism: more ocean–atmosphere heat transfer, higher SSTs, and a further and long-lasting northward retreat of the ice cover in the BS and, consequently, a thinner KS ice cover, accompanied with an earlier onset of melt and an increase of the length of the melt season as has been identified already by Rodrigues (2009).

Anomalies in the sea-ice export out of the Arctic Ocean via gates II and III (see Fig. 1) into regions BS and KS (Kwok, 2009) could also contribute to the observed BS and KS ice-area and -extent anomalies. In particular, enhanced import of sea ice into region BS might balance the effect of an oceanic heat anomaly by ice-melt induced strengthening of the surface water layer stratification and thus isolation of surface waters from the heat anomaly (Gerdes et al., 2003). Similar to regions GS and IS we compared winter (October–May) and summer (June–September) ice-area flux estimates into regions BS (gate II) and KS (gate III) with BS and KS ice-area and -extent anomalies by means of a lag-correlation [see Fig. 1 for location of gates II and III and Figs. 12b and c) for observed ice-area flux values between 1991/1992 and 2006/2007 according to Kwok (2009)]. The results are given in Table 6 and indicate significant correlations ($p \leq 0.05$, 95 % significance) between ice-area fluxes through gates II or III and BS and KS ice-area and -extent anomalies for both summer and winter, however with different time lags.

For gate II the highest correlation ($R = 0.57$) is observed between Arctic Ocean ice export in one winter and BS ice-area and extent anomalies in the subsequent winter (1-yr lag). Significant correlations are also found for summer Arctic Ocean ice export and BS ice-area and -extent anomalies the subsequent winter and summer. For gate III the highest correlation ($R = 0.75$) is observed between Arctic Ocean ice export in one winter and BS ice-area and extent anomalies in the subsequent summer. Correlations with the same winter's BS ice-area and extent anomalies are also high ($R = 0.64$). Correlations for summer ice import are less important. If we relate Arctic Ocean ice export through gate III to KS ice-area and -extent anomalies we find a similar picture: the highest correlation ($R = 0.69$) exists between winter Arctic Ocean ice export and summer KS ice-cover anomalies. This is followed by winter Arctic Ocean ice export and winter KS ice-cover anomalies, however with a 1-yr time lag, and in contrast to region BS by summer Arctic Ocean ice export and summer KS ice-cover anomalies, also with 1-yr time lag.

Table 6. Results of a lag correlation between winter (October–May) and summer (June–September) ice-area fluxes through gates II and III (Figs. 12b and c) and BS, KS and WPS ice-area and ice-extent anomalies

	lag (yr)	*R*
Gate II, BS		
S2S	1,1	**0.52**, **0.50**
S2W	1,1	**0.56**, **0.51**
W2W	1,1	**0.57**, **0.57**
W2S	0,0	**0.52**, 0.50
Gate III, BS		
S2S	–,–	–,–
S2W	–1,–1	−0.46, −0.46
W2W	0,0	**0.65**, **0.63**
	1,1	0.46, 0.47
W2S	0,0	**0.76**, **0.74**
Gate III, KS		
S2S	1,1	**0.58**, **0.64**
S2W	1,2	0.47,**0.54**
W2W	–1,–1	**−0.56**, **−0.57**
	1,1	**0.63**, **0.58**
W2S	0,0	**0.68**, **0.69**
Gate II, WPS	lag (yr)	*R*
S2W	1,–	0.44,–
W2W	–,–	–,–
Gate III, WPS		
S2W	1,1	**0.61**, **0.61**
W2W	–,–	–,–

Notes: Given are the time lag and correlation coefficients *R* with a minimum significance level (*S*-level) of 90% (based on a permutation test with 10 000 members). Values for area and extent are separated by a comma. Acronyms S2S, S2W, W2W and W2S stand for correlations of data between summer, summer and winter, winter, and winter and summer, respectively. Correlations with a *S*-level of 95% or more are highlighted bold. Note that for WPS values for S2S and W2S are omitted.

It remains speculative to interpret these correlations in the context of a causal relationship, because the general atmospheric circulation can cause both at the same time: enhanced (reduced) Arctic Ocean ice export and a positive (negative) BS ice-cover anomaly. Particularly during winter local ice formation is likely to mimic any variation in winter Arctic Ocean ice export via gate II or III. During summer, however, ice imported through these gates could substantially contribute to the ice cover in regions BS and KS and by this directly impact ice-area and -extent anomalies. Interestingly above-mentioned correlations draw a different picture since summer BS and KS ice-area and -extent

anomalies are only correlated with the summer ice import with a 1-yr time lag (Table 6, S2S). Instead, winter ice import is linked to summer ice-cover anomalies the same year (Table 6, W2S). Although this could be indicative of the import of thick ice during winter, which takes longer to melt, causing a positive ice-area and -extent anomaly in summer, this winter ice import could simply have been the result of a general atmospheric circulation which has also favoured an above normal BS ice extent and which also takes longer to melt causing a positive ice-area and -extent anomaly the following summer.

It cannot be ruled out, however, that any positive (negative) ice-import anomaly can result in positive (negative) anomaly of the amount of melt water at the surface after summer melt, which could precondition both regions (BS or KS) for the subsequent freezing period and which could suppress (favour) enhanced ocean-atmosphere heat transfer. Largest ice import via gate II occurred in winters 1995/96 and 2002/2003 (Figs. 12b). At the same time ice export out of regions KS and BS into the Arctic Ocean via gate III changed sign, becoming an ice import (Fig. 12c). These winters mark in fact the beginning of two about 1-yr long periods with positive BS ice-area and -extent anomalies (Figs. 6g and h). However, in winter 1998/1999 ice was exported out of BS and KS via both gate II and III (Figs. 12b and c); still a pronounced positive BS ice-area and -extent anomaly can be observed. Anomalies switched sign in winter 1999/2000, when gate III experienced the largest ice export out of KS and BS during the period 1992–2008.

Note that a significant anti-correlation is observed between winter Arctic Ocean ice export and winter KS ice-cover anomalies with minus 1-yr time lag. Since the flux is counted positive when directed out of the Arctic Ocean this anticorrelation means that a large winter ice-area import into the Arctic Ocean via gate III is associated with an above normal ice cover in the KS during the preceding winter. One example for this relationship is given by years 1998–2000: positive KS ice-area and -extent anomalies during 1998 and 1999 (Figs. 6j–l) coincide with maximum winter ice import into the Arctic Ocean via gate III in 1999 and 2000 (Fig. 12c). BS ice-cover anomalies were also positive in 1998 and 1999 (Figs. 6g–i) but a similar anticorrelation is not observed.

4.4. Interaction GS–BS

How can we explain the apparent relationship between GS and BS ice-area and -extent anomalies indicated in Fig. 11? These two regions are not directly linked to each other in terms of interregional ice transport as regions GS and IS are. The GS ice cover is strongly influenced by ice import out of the Arctic through Fram Strait with local ice formation probably playing a secondary role in the absence of an Is Odden. In contrast the BS ice cover is dominated by local ice formation which onset and duration seems however being influenced by the net import of sea ice out of the Arctic Ocean. The average (1979–2007) picture is (Kwok, 2009): sea ice is imported in the western BS (Fig. 1, gate II), while it is exported in the eastern BS (Fig. 1, gate III). This picture does not change for 1992–2007 (see Figs. 12b and c).

Table 7. Results of a lag correlation between ice-area fluxes through gates I, II and III (Fig. 12)

Gates	lag (yr)	*R*	*S*-level
I–II	1	0.54	90%
I–III	0	−0.53	90%
II–III	0	**0.64**	95%

Notes: Given are the peak correlation coefficients *R* and the significance level (*S*-level) obtained with a permutation test with 10 000 members. Values with an *S*-level below 68% are omitted. *R*-values with an *S*-level of 95% or above are highlighted bold.

A lag-correlation analysis is carried out between winter (October–May) ice-area fluxes through gates I, II and III (Fig. 12). The results (Table 7) indicate: (i) ice-area fluxes through gates II and III are significantly correlated; (ii) ice-area fluxes through gates I and III are anticorrelated; (iii) ice-area fluxes through gates I and II are correlated with 1 yr time lag. So, ice-area fluxes through gates II and III vary in phase and those through gates I and II are (with 90% significance) correlated with 1 yr time lag. Therefore we suggest that a winter with a high (low) ice-area export through Fram Strait is followed by a winter (or even a year) with a high (low) ice-area export into the BS and subsequently a positive (negative) BS ice-cover anomaly. We have demonstrated with Table 6, that BS ice-area and -extent anomalies do not respond immediately to enhanced (reduced) ice import out of the Arctic (if they respond at all, see discussion related to Table 6 in the last section) but with up to a year time lag. Therefore the large time lag and long-lasting correlation between GS and BS ice-area and -extent anomalies shown in Figs. 11a and b) seem reasonable.

5. Summary and conclusions

We examined the sea-ice cover of the Arctic peripheral seas bordering the Northern North Atlantic: IS, GS, BS, KS and WPS using daily sea-ice concentration data obtained with the ASI algorithm at a grid resolution of 12.5 km × 12.5 km from 85 GHz brightness temperature measurements. The obtained annual cycles of monthly average ice area and extent indicate an increase of the length of the melt season and reductions in the mean maximum and minimum ice-cover in all regions between 1992–1999 and 2000–2008, with winter-time changes of between 5–10% (GS, WPS) and 15–20% (IS, BS), and summer-time changes between 30% (KS) and up to 55% (IS, BS). This agrees with findings by Rodrigues (2009, 2008); Parkinson and Cavalieri (2008). Tables 8 and 9 summarize the results of a lag-correlation analysis between ice-area and -extent

Table 8. Maximum lag correlation coefficients *R* of monthly ice-area (top) and -extent (bottom) anomalies of regions: Irminger (IS), Greenland (GS), Barents (BS), Kara (KS) and White/Pechora Seas for 1992–2008, together with the start month and the time lag in parenthesis

	IS	GS	BS	KS	WPS
Area					
IS	**0.88** (Jan.+2)	**0.87** (Aug.+3)	–	–	–
GS	–	**0.92** (Sep.+1)	–	–	–
BS	–	–	**0.81** (Oct.+0)	**0.93** (Jul.+1)	**0.88** (Jan.+6)
WPS	–	–	**0.85** (Apr.+1)	**0.88** (Nov.+0)	**0.89** (Mar.+2)
Extent					
IS	**0.91** (Jan.+2)	**0.85** (Aug.+2)	–	–	–
GS	–	**0.93** (Aug.+1)	–	–	–
BS	–	0.76 (Feb.+20)	**0.95** (May+1)	0.75 (Oct.+0)	**0.86** (Jan.+4)
KS	–	–	0.75 (Oct.+0)	**0.94** (Jun.+1)	**0.82** (Jan.+7)
WPS	–	–	**0.86** (May+1)	**0.82** (Nov.+1)	**0.77** (Feb.+4)

Note: The diagonal (off-diagonal) elements show the autocorrelation (cross-correlation) for a time-lag >0. Pairs without a significant (≥95%) correlation are omitted. Correlations that are significant at 99% are highlighted bold.

Table 9. Average and maximum (in parentheses) duration in months of auto- (diagonal elements) and cross-correlations (all significant at ≥95%) of ice-area (top) and -extent (bottom) anomalies (compare Figs. 7–11)

	IS	GS	BS	KS	WPS
Area					
IS	2 (5)	2 (8)	–	–	–
GS	–	3 (4)	–	–	–
BS	–	3 (12)	7 (15)	1 (4)	3 (10)
KS	–	–	3 (5)	3 (6)	2 (9)
WPS	–	–	2 (4)	1 (2)	3 (6)
Extent					
IS	3 (7)	2 (8)	–	–	–
GS	–	3 (5)	–	–	–
BS	–	3 (10)	6 (10)	1 (3)	2 (10)
KS	–	–	2 (3)	3 (5)	2 (6)
WPS	–	–	2 (4)	1 (3)	3 (6)

Note: A value of one means that the correlation only includes the reference month.

anomalies. The main results are: (i) BS ice-area and -extent anomalies are autocorrelated for a two-fold longer period than respective anomalies in the other regions. (ii) Fall/early winter IS ice-area and -extent anomalies are significantly correlated with respective summer/fall GS anomalies; the average time-lag is 2–3 months, the average (maximum) duration of this correlation is 2 (8) months. No significant correlation is obtained between wintertime GS and IS ice-area and -extent anomalies. (iii) BS and KS ice-area and -extent anomalies are significantly correlated with each other during summer/fall. We found further a significant correlations between December to July BS and July to September/November KS ice-area and -extent anomalies with an average duration of 2–3 months. (iv) Jan. WPS ice-area and -extent anomalies are significantly correlated with respective BS and KS anomalies; maximum correlations occur with May (BS) and July/August (KS).

Correlations of ice-cover anomalies in and between regions GS and IS can be related to ice advection along the Greenland coast, and the export of sea ice through Denmark Strait. Evidently GS (summer) and IS (winter) ice-area and extent anomalies are linked to Fram Strait ice-area flux anomalies. We surmise that one reason for the GS ice-area and -extent decrease can be the fewer and less pronounced Is Odden events during 2000–2008 than 1992–2008. Fram Strait ice-area and -volume fluxes seem not have to played a significant role for the observed IS and GS ice-cover decrease since both fluxes have not changed significantly since the 1990s (Kwok, 2009; Spreen et al., 2009). Once the ice-volume import will decrease, however, it is likely that predominantly the summer GS ice cover will further decrease, and that as consequence of this the length of the ice-free season in region IS will further increase while ice area and extent will decrease. It is very important in this context to further improve sea-ice concentration algorithms for their capability to correctly calculate ice concentrations in the vicinity of coasts (see Fig. 4). One such an improvement is presented by Maass and Kaleschke (2010).

It is speculative to draw conclusions about the links between regions BS and KS as well as GS and BS that are suggested by our correlation analysis of ice-area and extent anomalies and between these and ice-area flux anomalies. This is because the observed correlations can in principle be the result of just one physical interaction process, such as the local ocean–ice–atmosphere feedback mechanism, but the characteristics of this mechanism are determined by the current and preceding large-scale atmospheric circulation which has a profound impact on the oceanic

heat content in the Nordic Seas as well as on the ice import into our regions of interest out of the Arctic Ocean (Sorteberg and Kvingedal, 2006; Deser and Teng, 2008; Zhang et al., 2008; Kwok, 2009).

However, we believe that results of such a correlation analysis could be useful to better interpret and understand the observed ice-area and -extent changes, and to suggest how the sea-ice cover in the Nordic Seas will develop in the future. We surmise that the ice-cover in region BS will be further reduced in the future, because of the depletion of the eastern Arctic Ocean of old ice (Nghiem et al., 2006) and thus less import of thick ice into region BS, and because of the recent increase of cyclonic activity in the northern North Atlantic and region BS and the associated oceanic heat anomalies (Zhang et al., 2008). This already has an impact on the KS ice cover, but our results suggests also that region WPS could exert a stabilizing influence since (i) its maximum wintertime ice cover has remained much more stable than that in region BS and (ii) WPS wintertime ice-area and -extent anomalies are positively and significantly correlated with respective anomalies in region KS.

The BS ice cover interacts, as part of a positive feedback loop in the ocean-ice-atmosphere interaction with the BSI (Bengtsson et al., 2004; Semenov et al., 2009). This inflow has been recently suggested to have larger impact on the intermediate Atlantic Water (AW) layer in the Arctic Ocean, particularly beyond the Nansen Basin (Dmitrenko et al., 2009; Dickson, 2009). Therefore, a continuation of the observed BS ice-cover decrease and thus enhanced BSI could also have implications on the characteristics of the AW layer in the western Arctic Ocean.

6. Acknowledgments

Satellite data provision by the National Snow and Ice Data Centre (NSIDC), Boulder, Co, USA, and provision of the operational ice-concentration maps by CERSAT/IFREMER, Brest, France is greatly acknowledged. Thanks go the Carmen Ulmen, CLISAP, University of Hamburg, Hamburg, Germany, for median-filtering of the ASI data. This work has been funded by the German Science Foundation (DFG) via SFB512, Teilprojekt E1 and E5. The authors also wish to thank two anonymous reviewers whose comments together with those of the editor helped to substantially improve the manuscript.

References

Aagaard, E. and Carmack, E. C. 1989. The role of sea ice and other fresh water in the Arctic circulation. *J. Geophys. Res.* **94**(C10), 14485–14498.

ACIA 2005. *Arctic Climate Impact Assessment*. (ed. C. Symon), Cambridge University Press, Cambridge, UK, 1042p, http://www.acia.uaf.edu.

Andersen, S., Tonboe, R., Kaleschke, L., Heygster, G. and Pedersen, L. T. 2007. Intercomparison of passive microwave sea ice concentration retrievals over the high-concentration Arctic sea ice. *J. Geophys. Res.* **112**(C8), C08004, doi:10.1029/2006JC003543.

Arrigo, K. R., van Dijken, G. and Pabi, S. 2008. Impact of a shrinking Arctic ice cover on marine primary production. *Geophys. Res. Lett.* **35**, L19603, doi:10.1029/2008GL035028.

Bengtsson, L., Semenov, V. A. and Johannessen, O.M. 2004. The early twentieth-century warming in the Arctic: a possible mechanism. *J. Clim.* **17**(20), 4045–4057.

Cavalieri, D. J., St. Germain, K. M. and Swift, C. T. 1995. Reduction of weather effects in the calculation of sea-ice concentration with DMSP SSM/I. *J. Glaciol.* **41**(139), 455–464.

Comiso, J. C 1999. Bootstrap sea ice concentrations from NIMBUS-7 SMMR and DMSP SSM/I (01/1992-12/2007). *National Snow and Ice Data Centre, Boulder, Colorado, U.S.A., Digital Media.*.

Comiso, J., Cavalieri, D. J., Parkinson, C. L. and Gloersen, P. 1997. Passive microwave algorithms for sea ice concentration: a comparison of two techniques. *Remote Sens. Environ.* **60**(3), 357–384.

Comiso, J. C., Wadhams, P., Pedersen, L. T. and Gersten, R.A. 2001. Seasonal and interannual variability of the Odden ice tongue and a study of environmental effects. *J. Geophys. Res.* **106**(C5), 9093–9116.

Comiso, J., Parkinson, C. L., Gersten, R. and Stock, L. 2008. Accelerated decline in the Arctic sea ice cover. *Geophys. Res. Lett.* **35**, L01703, doi:10.1029/2007GL031972.

Deser, C. and Teng, H. 2008. Evolution of Arctic sea ice concentration trends and the role of atmospheric circulation forcing, 1979-2007. *Geophys. Res. Lett.* **35**, L02504, doi:10.1029/2007GL032023.

Deshayes, J., Frankignoul, C. and Drange, H. 2007. Formation and export of deep water in the Labrador and Irminger Seas in a GCM. *Deep Sea Res. I* **54**, 510–532.

Dickson, B. 2009. Securing the legacy of the IPY. *Nat. Geosci.* **2**(6), 374–376.

Dickson, B., Meincke, J., Malmberg, S.-A. and Lee, A. J. 1988. The "Great Salinity Anomaly" in the northern north Atlantic 1968-1982. *Prog. Oceanogr.* **20**(2), 103–151.

Dickson, B., Osborn, T. J., Hurrell, J. W., Meincke, J., Blindheim, J. and co-authors. W. 2000. The Arctic Ocean response to the North Atlantic Oscillation. *J. Clim.* **13**(15), 2671–2696.

Dickson, B., Rudels, B., Dye, S., Karcher, M., Meincke, J. and co-authors. 2007. Current estimates of freshwater flux through Arctic and subarctic seas. *Prog. Oceanogr.* **73**(3-4), 210–230.

Dmitrenko, I. A., Kirillov, S. A., Ivanov, V. V., Woodgate, R. A., Polyakov, I. V. and co-authors. 2009. Seasonal modification of the Arctic Ocean intermediate water layer off the esatern Laptev Sea continental shelf break. *J. Geophys. Res.* **114**, C06010, doi:10.1029/2008JC005229.

Divine, D. V. and Dick, C. 2006. Historical variability of sea ice edge position in the Nordic Seas. *J. Geophys. Res.* **111**, C01001, doi:10.1029/2004JC002851.

Francis, J. A. and Hunter, E. 2006. New insights into the disappearing Arctic sea ice. *EOS, Trans. Amer. Geophys. Un.* **87**(46), 509–510.

Francis, J. A. and Hunter, E. 2007. Drivers of declining sea ice in the Arctic winter: a tale of two seas. *Geophys. Res. Lett.* **34**, L17503, doi:10.1029/2007GL030995.

Garrity, C., Lubin, D., Kern, S. and Pedersen, L. T. 2002. Linescan camera evaluation of SSM/I 85.5 GHz sea ice retrieval. *Remote Sens. Environ.* **83**(3), 472–487.

Gerdes, R., Karcher, M. J., Kauker, F. and Schauer, U. 2003. Causes and development of repeated Arctic Ocean warming events. *Geophys. Res. Lett.* **30**(19), 1980, doi:10.1029/2003GL018080.

Gloersen, P. and Cavalieri, D. 1986. Reduction of weather effects in the calculation of sea ice concentration from microwave radiances. *J. Geophys. Res.* **91**(C3), 3913–3919.

Gloersen, P., Campbell, W., Cavalieri, D., Comiso, J., Parkinson, C. and co-authors. 1992. Arctic and Antarctic sea ice, 1978-1987: Satellite Passive Microwave Observations and Analysis. In: *Scientific and Technical Information Program, vol. NASA SP-511*, (eds. P. Gloersen), National Aeronautical and Space Administration (NASA), Washington, DC, U.S.A., 284 pp.

Grenfell, T. C., Barber, D. G., Fung, A. K., Gow, A. J., Jezek, K. C. and co-authors. 1998. Evolution of electromagnetic signatures of sea ice from initial formation to the establishment of thick first-year ice. *Trans. Geosci. Remote Sens.* **36**(5), 1642–1654.

Haas, C., Pfaffling, A., Hendricks, S., Rabenstein, L., Etienne, J.-L. and co-authors. 2008. Reduced ice thickness in Arctic Transpolar Drift favors rapid ice retreat. *Geophys. Res. Lett.* **35**, L17501, doi:10.1029/2008GL034457.

Holfort, J. and Meincke, J. 2003. Time series of freshwater-transport on the East Greenland Shelf at 74°N. *Meteor. Z.* **14**(6), 703–710, doi:10.1127/0941-2948/2005/0079.

Jähne, B. 1997. *Digitale Bildverarbeitung*, Springer Verlag, Heidelberg, Germany, 591 pp.

Jungclaus, J. H.., Haack, H., Latif, M. and Mikolajewicz, U. 2005. Arctic-North Atlantic interactions and multidecadal variability of the meridional overturning circulation. *J. Clim.* **18**(19), 4013–4031.

Kaleschke, L., Lüpkes, C., Vihma, T., Haarpaintner, J., Bochert, A. and co-authors. 2001. SSM/I sea ice remote sensing for mesoscale ocean-atmosphere interaction analysis. *Can. J. Remote Sens.* **27**(5), 526–537.

Karstensen, J., Schlosser, P., Wallace, D. W. R., Bullister, J. L. and Blindheim, J. 2005. Water mass transformation in the Greenland Sea during the 1990s. *J. Geophys. Res.* **110**, C07022, doi:10.1029/2004JC002510.

Kern, S. 2004. A new method for medium-resolution sea ice analysis using weather-influence corrected Special Sensor Microwave/Imager 85 GHz data. *Int. J. Remote Sens.* **25**(21), 4555–4582.

Kern, S., Kaleschke, L. and Clausi, D. A. 2003. A comparison of two 85 GHz SSM/I ice concentration algorithms with AVHRR and ERS-2 SAR imagery. *Trans. Geosci. Remote Sens.* **41**(10), 2294–2306.

Kwok, R. 2009. Outflow of Arctic Ocean sea ice into the Greenland and Barents Seas: 1979-2007. *J. Clim.* **22**, 2438–2457, doi:10.1175/2008JCLI2819.1.

Kwok, R. and Rothrock, D. A. 2009. Decline in Arctic sea ice thickness from submarine and ICESat records: 1958–2008. *Geophys. Res. Lett.* **36**, L15501, doi:10.1029/2009GL039035.

Kwok, R., Cunningham, G. F. and Pang, S. S. 2004. Fram Strait sea ice outflow. *J. Geophys. Res.* **109**, C01009, doi:10.1029/2003JC001785.

Kwok, R., Maslowski, W. and Laxon, S. W. 2005. On large outflows of Arctic sea ice into the Barents Sea. *Geophys. Res. Lett.* **32**, L22503, doi:10.1029/2005GL024485.

Kwok, R., Cunningham, F., Wensnahan, M., Rigor, I., Zwally, H. J. and co-authors. 2009. Thinning and volume loss of the Arctic Ocean sea ice cover: 2003-2008. *J. Geophys. Res.* **114**, C07005, doi:10.1029/2009JC005312.

Latarius, K. and Quadfasel, D. 2010. A heat and freshwater budget of the Greenland Sea on seasonal to interannual scales. *Tellus 62A* this issue,

Maass, N. and Kaleschke, L. 2010. Validation of passive microwave algorithms applied to sea ice in coastal regions. *Tellus 62A* this issue,

Maslowski, W., Marble, D., Walczowski, W., Schauer, U., Clement, J. L. and co-authors. 2004. On climatological mass, heat, and salt transports through the Barents Sea and Fram Strait from a pan-Arctic coupled ice-ocean model simulation. *J. Geophys. Res.* **109**, C03032, doi:10.1029/2001JC001039.

Mysak, L.A. and Manak, D.K. 1989. Arctic Sea-ice Extent and Anomalies, 1953-1984. *Atmos. Ocean* **27**(2), 376–405.

Nghiem, S. V., Chao, Y., Neumann, G., Li, P., Perovich, D. K. and co-authors. 2006. Depletion of perennial sea ice in the East Arctic Ocean. *Geophys. Res. Lett.* **33**, L17501, doi:10.1029/2006GL027198.

NORSEX Group, 1983. Norwegian remote sensing experiment in a marginal ice zone. *Science* **220**(4599), 781–787.

Onstott, R. G., Grenfell, T. C., Mtzler, C., Luther, C. A. and Svendsen, E. A. 1987. Evolution of microwave sea ice signatures during early summer and midsummer in the marginal ice zone. *J. Geophys. Res.* **92**(C7), 6825–6835.

Parkinson, C. L. and Cavalieri, D. J. 2008. Arctic sea ice variability and trends, 1979-2006. *J. Geophys. Res.* **113**, C07003, doi:10.1029/2007JC004558.

Pfirman, S., Colony, R., Nürnberg, D., Eicken, H. and Rigor, I. 1997. Reconstructing the origin and trajectory of drifting Arctic sea ice. *J. Geophys. Res.* **102**(C6), 12 575–12 586.

Pfirman, S., Haxby, W. F., Colony, R. and Rigor, I. 2004. Variability in Arctic sea ice drift. *Geophys. Res. Lett.* **31**, L16402, doi:10.1029/2004GL020063.

Rampal, P., Weiss, J and Marsan, D. 2009. Positive trend in the mean speed and deformation rate of Arctic sea ice, 1979–2007. *J. Geophys. Res.* **114**, C05013, doi:10.1029/2008JC005066.

Rigor, I. and Wallace, J. M. 2004. Variations in the age of Arctic sea-ice and summer sea-ice extent. *Geophys. Res. Lett.* **31**, L09401, doi:10.1029/2004GL019492.

Rodrigues, J. 2006. Recent changes in the sea ice distribution in the Russian Arctic: ice extent, area and length of the ice-free season. In: *Arctic Sea Ice Thickness: Past, Present and Future*, (eds. P. Wadhams and G. Amanatidis), European Commission, Brussels, **EUR 22416**, 244–291, http://bookshop.europa.eu/uri?target=EUB:NOTICE:KINA22416:EN:HTML.

Rodrigues, J. 2008. The rapid decline of the sea ice in the Russian Arctic. *Cold Reg. Sci. Technol.*, **54**(2), 124–142, doi:10.1016/j.coldregions.2008.03.008.

Rodrigues, J. 2009. The increase in the length of the ice-free season in the Arctic. *Cold Reg. Sci. Technol.*, doi:10.1016/j.coldregions.2009.05.006.

Rogers, J. C. and Hung, M.-P. 2008. The Odden ice feature of the Greenland Sea and its association with atmospheric pressure, wind, and surface flux variability from reanalyses. *Geophys. Res. Lett.* **35**, L08504, doi:10.1029/2007GL032938.

Rysgaard, S., Bendtsen, J., Pedersen, L. T., Ramlov, H. and Glud, R. N. 2009. Increased CO2 uptake due to sea ice growth and decay in the Nordic Seas. *J. Geophys. Res.* **114**, C09011, doi:10.1029/2008JC005088.

Sachs, L. and Hedderich, J. 2006. *Angewandte Statistik - Methodensammlung mit R*, Springer Verlag, Heidelberg, Germany, 702 pp.

Schauer, U., Loeng, H., Rudels, B., Ozhigin, V. K. and Dieck, W. 2002. Atlantic water flow through the Barents and Kara Seas. *Deep Sea Res. I* **49**(12), 2281–2298.

Semenov, V.A., Park, W. and Latif, M. 2009. Barents Sea inflow shutdown: a new mechanism for rapid climate changes. *Geophys. Res. Lett.* **36**, L14709, doi:10.1029/2009GL038911.

Shokr, M., Asmus, K. and Agnew, T. A. 2009. Microwave emission observations from artificial thin sea ice: the ice-tank experiment. *Trans. Geosci. Remote Sens.* **47**(1), 325–338.

Shuchman, R. A., Josberger, E. G., Russel, C. A., Fischer, K.W., Johannessen, O. M. and co-authors. 1998. Greenland Sea Odden sea ice feature: intra-annual and interannual variability. *J. Geophys. Res.* **103**(C6), 12 709–12 724.

Sorteberg, A. and Kvingedal, B. 2006. Atmospheric forcing on the Barents Sea winter ice extent. *J. Clim.* **19**, 4772–4784.

Spreen, G., Kaleschke, L. and Heygster, G. 2008. Sea ice remote sensing using AMSR-E 89 GHz channels. *J. Geophys. Res.* **113**, C02S03, doi:10.1029/2005JC003384.

Spreen, G., Kern, S., Stammer, D. and Hansen, E. 2009. Fram Strait sea ice volume export estimated between 2003 and 2008 from satellite data. *Geophys. Res. Lett.*, **36**, L19502, doi:10.1029/2009GL039591.

Sundfjord, A., Ellingsen, I., Slagstad, D. and Svendsen, H. 2008. Vertical mixing in the marginal ice zone of the northern Barents Sea—results from numerical modeling experiments. *Deep Sea Res. II* **55**, 2154–2168.

Svendsen, E., Mätzler, C. and Grenfell, T. C. 1987. A model for retrieving total sea ice concentration from a space-borne passive microwave instrument operating near 90 GHz. *Int. J. Remote Sens.* **8**(10), 1479–1487.

Vinje, T. 2001. Anomalies and Trends of Sea-Ice Extent and Atmospheric Circulation in the Nordic Seas during the Period 1864-1998. *J. Clim.* **14**(3), 255–267, doi:10.1175/1520-0442(2001)0140255:AATOSI>2.0.CO;2.

Visbeck, M., Fischer, J. and Schott, F. 1995. Preconditioning the Greenland Sea for deep convection: ice formation and ice drift. *J. Geophys. Res.* **100**(C9), 18 489–18 502.

Wilkinson, J. P. and Wadhams, P. 2003. A salt flux model for salinity change through ice production in the Greenland Sea and its relationship to winter convection. *J. Geophys. Res.* **108**(C5), 3147, doi:10.1029/2001JC001099.

Winsor, P. and Björk, G. 2000. Polynya activity in the Arctic Ocean from 1958 to 1997. *J. Geophys. Res.* **105**(C4), 8789–8803.

Zhang, X., Sorteberg, A., Zhang, J., Gerdes, R. and Comiso, J. C. 2008. Recent radical shifts of atmospheric circulations and rapid changes in Arctic climate system. *Geophys. Res. Lett.* **35**, L22701, doi:10.1029/2008GL035607.